

**Meson-baryon scattering lengths from mixed-action lattice QCD**A. Torok,<sup>1</sup> S. R. Beane,<sup>1</sup> W. Detmold,<sup>2,3</sup> T. C. Luu,<sup>4</sup> K. Orginos,<sup>2,3</sup> A. Parreño,<sup>5</sup> M. J. Savage,<sup>6</sup> and A. Walker-Loud<sup>2</sup>

(NPLQCD Collaboration)

<sup>1</sup>*Department of Physics, University of New Hampshire, Durham, New Hampshire 03824-3568, USA*<sup>2</sup>*Department of Physics, College of William and Mary, Williamsburg, Virginia 23187-8795, USA*<sup>3</sup>*Jefferson Laboratory, 12000 Jefferson Avenue, Newport News, Virginia 23606, USA*<sup>4</sup>*N Division, Lawrence Livermore National Laboratory, Livermore, California 94551, USA*<sup>5</sup>*Departament d'Estructura i Constituents de la Matèria and Institut de Ciències del Cosmos, Universitat de Barcelona, E-08028 Barcelona, Spain*<sup>6</sup>*Department of Physics, University of Washington, Seattle, Washington 98195-1560, USA*

(Received 27 October 2009; published 26 April 2010)

The  $\pi^+\Sigma^+$ ,  $\pi^+\Xi^0$ ,  $K^+p$ ,  $K^+n$ , and  $\bar{K}^0\Xi^0$  scattering lengths are calculated in mixed-action Lattice QCD with domain-wall valence quarks on the asqtad-improved coarse MILC configurations at four light-quark masses, and at two light-quark masses on the fine MILC configurations. Heavy-baryon chiral perturbation theory with two and three flavors of light quarks is used to perform the chiral extrapolations. To the order we work in the three-flavor chiral expansion, the kaon-baryon processes that we investigate show no signs of convergence. Using the two-flavor chiral expansion for extrapolation, the pion-hyperon scattering lengths are found to be  $a_{\pi^+\Sigma^+} = -0.197 \pm 0.017$  fm, and  $a_{\pi^+\Xi^0} = -0.098 \pm 0.017$  fm, where the comprehensive error includes statistical and systematic uncertainties.

DOI: 10.1103/PhysRevD.81.074506

PACS numbers: 12.38.Gc

**I. INTRODUCTION**

Lattice QCD calculations of meson-meson interactions have yielded predictions for physical scattering lengths at the few percent level [1–3]. Several reasons underlie this striking accuracy. Firstly, at the level of the lattice calculation, Euclidean-space correlation functions involving pseudoscalar mesons have signal/noise ratios<sup>1</sup> that do not degrade, or only slowly degrade with time. Therefore, highly accurate fits of both single- and multimeson properties are possible with currently available supercomputer resources. Recent calculations of multimeson interactions relevant for the study of pion and kaon condensation have been performed with up to 12 mesons interacting on a lattice [4–6] with no appreciable degradation of signal/noise with time. Secondly, and perhaps more importantly, QCD correlation functions involving Goldstone bosons are subject to powerful chiral symmetry constraints. Since current lattice calculations are carried out at unphysical quark masses, these constraints play an essential role in extrapolating the lattice data to the physical quark masses, as well as to the infinite volume, and continuum limits. Chiral perturbation theory ( $\chi$ -PT) is the optimal method for implementing QCD constraints due to chiral symmetry, and in essence, provides an expansion of low-energy S-matrix elements in quark masses and powers of momentum [7].

<sup>1</sup>Here the signal is the Monte Carlo estimate of the quantum correlation function evaluated on the lattice, while the noise represents the statistical fluctuations in the correlation function.

In contrast to the purely mesonic sector, recent studies of baryon-baryon interactions, the paradigmatic nuclear physics process, have demonstrated the fundamental difficulty faced in making predictions for baryons and their interactions [8,9]. Unlike the mesons, correlation functions involving baryons suffer an exponential degradation of signal/noise at large times<sup>2</sup> and therefore pose a fundamentally different kind of challenge in extracting signal from data [11]. Furthermore, while baryon interactions are constrained by QCD symmetries like chiral symmetry, the constraints are not nearly as powerful as when there is at least one pion or kaon in the initial or final state. For instance, there is no expectation that the baryon-baryon scattering lengths vanish in the chiral limit as they do in the purely mesonic sector. In nucleon-nucleon scattering, the *s*-wave interactions are actually enhanced due to the close proximity of a nontrivial fixed point of the renormalization group, which drives the scattering lengths to infinity, thus rendering the effective field theory description of the interaction highly nonperturbative [12].

Given the contrast in difficulty between the purely mesonic and purely baryonic sectors described above, it is clearly of great interest to perform a lattice QCD investigation of the simplest scattering process involving at least one baryon: meson-baryon scattering. While pion-nucleon

<sup>2</sup>A recent high-statistics study of baryon correlation functions on anisotropic clover lattices has found that the exponential decay with time of signal/noise occurs only *asymptotically* in time, and therefore, the signal/noise problem in baryon correlation functions is not nearly as severe as previously thought [10].

scattering is the best-studied process, both theoretically and experimentally, its determination on the lattice is computationally prohibitive since it involves annihilation diagrams. At present only a few limiting cases that involve these diagrams are being investigated [13]. Combining the lowest-lying  $SU(3)$  meson and baryon octets, one can form five meson-baryon elastic-scattering processes that do not involve annihilation diagrams. Three of these involve kaons and therefore are, in principle, amenable to an  $SU(3)$  heavy-baryon  $\chi$ -PT (HB $\chi$ -PT) analysis [14] for extrapolation. The remaining two processes involve pions interacting with hyperons and therefore can be analyzed in conjunction with the kaon processes in  $SU(3)$  HB $\chi$ -PT, or independently using  $SU(2)$  HB $\chi$ -PT.

Meson-baryon scattering has been developed to several nontrivial orders in the  $SU(3)$  HB $\chi$ -PT expansion in Refs. [15,16], extending earlier work on kaon-nucleon scattering in Ref. [17]. A very recent paper [18] has reconsidered the  $SU(3)$  HB $\chi$ -PT results using a different regularization scheme, and also derived results for pion-hyperon scattering in the  $SU(2)$  HB $\chi$ -PT expansion. These works make clear that the paucity of experimental data make it is very difficult to assess the convergence of the chiral expansion in the three-flavor case. Further, in the pion-hyperon system, the complete lack of experimental data precludes a separate analysis in the chiral two-flavor expansion. A lattice calculation of meson-baryon scattering analyzed using  $\chi$ -PT is therefore useful not only in making predictions for low-energy scattering at the physical point, but also for assessing the convergence of the chiral expansion for a range of quark masses at which present-day lattice calculations are being performed.

Meson-baryon scattering is also of interest for several indirect reasons. The  $K^-n$  interaction is important for the description of kaon condensation in the interior of neutron stars [19], and meson-baryon interactions are essential input in determining the final-state interactions of various decays that are interesting for standard-model phenomenology (See Ref. [20] for an example). Finally, in determining baryon excited states on the lattice, it is clear that the energy levels that represent meson-baryon scattering on the finite-volume lattice must be resolved before progress can be made regarding the extraction of single-particle excitations.

The experimental input to existing  $\chi$ -PT analyses of meson-baryon scattering is extensively discussed in Refs. [15–18]. Threshold pion-nucleon scattering information is taken from experiments with pionic hydrogen and deuterium [21,22], and the kaon-nucleon scattering lengths are taken from model-dependent extractions from kaon-nucleon scattering data [23]. There is essentially no experimental information available on the pion-hyperon and kaon-hyperon scattering lengths. There have been two quenched lattice QCD studies of meson-baryon scattering parameters: the pioneering work of Ref. [24] calculated

pion-nucleon and kaon-nucleon scattering lengths at heavy pion masses without any serious attempt to extrapolate to the physical point, and Ref. [25] calculated the  $I = 1$   $KN$  scattering length and found a result consistent with the current algebra prediction.

In this work we calculate the lowest-lying energy levels for five meson-baryon processes that have no annihilation diagrams:  $\pi^+\Sigma^+$ ,  $\pi^+\Xi^0$ ,  $K^+p$ ,  $K^+n$ , and  $\bar{K}^0\Xi^0$  in a mixed-action Lattice QCD calculation with domain-wall valence quarks on the asqtad-improved coarse MILC configurations with  $b \sim 0.125$  fm at four light-quark masses ( $m_\pi \sim 291, 352, 491$  and  $591$  MeV), and at two light-quark masses ( $m_\pi \sim 320$  and  $441$  MeV) on the fine MILC configurations with  $b \sim 0.09$  fm, with substantially less statistics on the fine ensembles. We extract the  $s$ -wave scattering lengths from the two-particle energies, and analyze the five processes using  $SU(3)$  HB $\chi$ -PT. We find a rather conclusive lack of convergence in the three-flavor chiral expansion. We then consider  $\pi^+\Sigma^+$  and  $\pi^+\Xi^0$  using  $SU(2)$  HB $\chi$ -PT and find that we are able to make reliable predictions of the scattering lengths at the physical point. We find

$$a_{\pi^+\Sigma^+} = -0.197 \pm 0.017 \text{ fm}; \quad (1)$$

$$a_{\pi^+\Xi^0} = -0.098 \pm 0.017 \text{ fm}, \quad (2)$$

where the errors encompass statistical and systematic uncertainties. The leading order  $\chi$ -PT (current algebra) predictions for the scattering lengths are given by [26]:

$$a_{\pi^+\Sigma^+} = -0.2294 \text{ fm}; \quad (3)$$

$$a_{\pi^+\Xi^0} = -0.1158 \text{ fm}. \quad (4)$$

Ultimately, either the chiral extrapolation should be performed after a continuum limit has been taken, or one should use the mixed-action extension of HB $\chi$ -PT to perform the chiral extrapolations [27,28]. However, our results on the fine MILC configurations are statistics-limited and not yet sufficiently accurate to make this a useful exercise. Further, the explicit extrapolation formulas for the meson-baryon scattering lengths have not yet been determined in mixed-action  $\chi$ -PT. Despite these limitations, we expect the corrections from finite lattice spacing to be small for two principle reasons. Firstly, the meson-baryon scattering lengths are protected by chiral symmetry and therefore the (approximate) chiral symmetry of the domain wall valence fermions used in this work protects the scattering lengths from additive renormalization, which can be explicitly seen in the construction of the mixed-action baryon Lagrangian in Ref. [28]. The mixed-action corrections do not appear until next-to-next-to leading order in the chiral expansion of the meson-baryon scattering lengths. Secondly, our previous experience with this mixed-action lattice QCD program leads us to expect that discretization effects will be well-encompassed within the

overall errors we quote. In our precise calculation of meson-meson scattering, the predicted mixed-action corrections [29,30] were smaller than the uncertainties on a given ensemble [1,3].

This paper is organized as follows. In Sec. II we isolate the five meson-baryon processes with no annihilation diagrams that are calculated in this work. We briefly review the standard Lüscher method for extracting the scattering amplitude from two-particle energy levels in a finite volume in Sec. III. Particulars regarding the mixed-action lattice calculation and fitting methods are provided in Sec. IV. Additional details can be found in Ref. [31]. Mixing between two of the meson-baryon channels with the same quantum numbers is discussed in Sec. V. In Sec. VI we consider chiral extrapolations of the lattice data using  $SU(3)$  HB $\chi$ -PT, and in Sec. VII we analyze the pion-hyperon lattice data using  $SU(2)$  HB $\chi$ -PT. Finally, we conclude in Sec. VIII.

## II. MESON-BARYON SCATTERING PROCESSES

It is a straightforward exercise to construct the six scattering channels involving the lowest-lying octet mesons and baryons that do not have annihilation diagrams, and to determine their isospin.<sup>3</sup> The particle content, isospin, and valence-quark content of these meson-baryon states are shown in Table I. We adopt the notation of Ref. [15], denoting the threshold  $T$ -matrix in the isospin basis as  $T_{\phi B}^{(I)}$ , where  $I$  is the isospin of the meson-baryon combination,  $\phi$  is the meson, and  $B$  is the baryon. The five elastic meson-baryon scattering processes that we consider are then in correspondence with the isospin amplitudes according to

$$T_{\pi^+\Sigma^+} = T_{\pi\Sigma}^{(2)}; \quad T_{\pi^+\Xi^0} = T_{\pi\Xi}^{(3/2)}; \quad T_{K^+p} = T_{KN}^{(1)}; \\ T_{K^+n} = \frac{1}{2}(T_{KN}^{(1)} + T_{KN}^{(0)}); \quad T_{\bar{K}^0\Xi^0} = T_{\bar{K}\Xi}^{(1)}. \quad (5)$$

These threshold  $T$ -matrices are related to the scattering lengths  $a_{\phi B}$  through

$$T_{\phi B} = 4\pi \left(1 + \frac{m_\phi}{m_B}\right) a_{\phi B}, \quad (6)$$

where  $m_\phi$  is the meson mass and  $m_B$  is the baryon mass.

## III. FINITE-VOLUME CALCULATION OF SCATTERING AMPLITUDES

The  $s$ -wave scattering amplitude for two particles below inelastic thresholds can be determined using Lüscher's method [32], which entails a measurement of one or

<sup>3</sup>The  $\pi^+\Xi^0$  and  $\bar{K}^0\Sigma^+$  systems have the same quantum numbers, and therefore require a mixed-channel analysis in order to extract the  $\bar{K}^0\Sigma^+$  scattering length. This is discussed in Section V.

TABLE I. Particle content, isospin, and valence-quark structure of the meson-baryon states calculated in this work. As is clear from the valence-quark content, these meson-baryon states have no annihilation diagrams.

Particles	Isospin	Quark Content
$\pi^+\Sigma^+$	2	$uu\bar{d}s$
$\pi^+\Xi^0$	3/2	$uu\bar{d}ss$
$K^+p$	1	$uuud\bar{s}$
$K^+n$	0 and 1	$uudd\bar{s}$
$\bar{K}^0\Sigma^+$	3/2	$uu\bar{d}ss$
$\bar{K}^0\Xi^0$	1	$u\bar{d}sss$

more energy levels of the two-particle system in a finite volume. For two particles with masses  $m_\phi$  and  $m_B$  in an  $s$ -wave, with zero total three momentum, and in a finite volume, the difference between the energy levels and those of two noninteracting particles can be related to the inverse scattering amplitude via the eigenvalue equation [32]

$$p \cot\delta(p) = \frac{1}{\pi L} \mathbf{S}\left(\frac{pL}{2\pi}\right), \quad (7)$$

where  $\delta(p)$  is the elastic-scattering phase shift, and the regulated three-dimensional sum is

$$\mathbf{S}(\eta) \equiv \sum_{\mathbf{j}}^{|j|<\Lambda} \frac{1}{|\mathbf{j}|^2 - \eta^2} - 4\pi\Lambda. \quad (8)$$

The sum in Eq. (8) is over all triplets of integers  $\mathbf{j}$  such that  $|\mathbf{j}| < \Lambda$  and the limit  $\Lambda \rightarrow \infty$  is implicit [33]. This definition is equivalent to the analytic continuation of zeta-functions presented by Lüscher [32]. In Eq. (7),  $L$  is the length of the spatial dimension in a cubically-symmetric lattice. The energy eigenvalue,  $E_n$ , and its deviation from the sum of the rest masses of the particle,  $\Delta E_n$ , are related to the center-of-mass momentum  $p_n$ , a solution of Eq. (7), by

$$\Delta E_n \equiv E_n - m_\phi - m_B \\ = \sqrt{p_n^2 + m_\phi^2} + \sqrt{p_n^2 + m_B^2} - m_\phi - m_B; \\ = \frac{p_n^2}{2\mu_{\phi B}} + \dots, \quad (9)$$

where  $\mu_{\phi B}$  is the reduced mass of the meson-baryon system. In the absence of interactions between the particles,  $|p \cot\delta| = \infty$ , and the energy levels occur at momenta  $\mathbf{p} = 2\pi\mathbf{j}/L$ , corresponding to single-particle modes in a cubic cavity with periodic boundary conditions. Expanding Eq. (7) about zero momenta,  $p \sim 0$ , one obtains the familiar relation<sup>4</sup>

<sup>4</sup>In order to be consistent with the meson-baryon literature, we have chosen to use the ‘‘particle physics’’ definition of the scattering length, as opposed to the ‘‘nuclear physics’’ definition, which is opposite in sign.

$$\Delta E_0 = -\frac{2\pi a}{\mu_{\phi B} L^3} \left[ 1 + c_1 \frac{a}{L} + c_2 \left( \frac{a}{L} \right)^2 \right] + \mathcal{O}\left(\frac{1}{L^6}\right), \quad (10)$$

with

$$c_1 = \frac{1}{\pi} \sum_{\substack{|\mathbf{j}| < \Lambda \\ \mathbf{j} \neq 0}} \frac{1}{|\mathbf{j}|^2} - 4\Lambda = -2.837297, \quad (11)$$

$$c_2 = c_1^2 - \frac{1}{\pi^2} \sum_{\substack{|\mathbf{j}| < \Lambda \\ \mathbf{j} \neq 0}} \frac{1}{|\mathbf{j}|^4} = 6.375183,$$

and  $a$  is the scattering length, defined by

$$a = \lim_{p \rightarrow 0} \frac{\tan \delta(p)}{p}. \quad (12)$$

As the finite-volume lattice calculation cannot achieve  $p = 0$  (except in the absence of interactions), in quoting a lattice value for the scattering length extracted from the ground-state energy level, it is important to determine the error associated with higher-order range corrections.

#### IV. LATTICE CALCULATION AND DATA ANALYSIS

In calculating the meson-baryon scattering lengths, the mixed-action lattice QCD scheme was used in which domain-wall quark [34–38] propagators are generated from a smeared source on  $n_f = 2 + 1$  asqtad-improved [39,40] rooted, staggered sea quarks [41]. The masses of the pions computed with the domain-wall propagators in this study are equal within a few percent to those of the lightest, staggered pions computed from staggered propagators that were generated with the same parameters as the given MILC gauge configuration [42]. This process has been done in several other mixed-action studies by NPLQCD and by LHP [43]. To improve the chiral symmetry properties of the domain-wall quarks, hypercubic-smearing (HYP-smearing) [44–46] was used in the gauge links of the valence-quark action. In the sea-quark sector, there has been significant debate regarding the validity of taking the fourth root of the staggered fermion determinant at finite lattice spacing [47–60]. While there is no proof, there are arguments to suggest that taking the fourth root of the fermion determinant recovers the contribution from a single Dirac fermion. The results of this paper assume that the fourth-root trick recovers the correct continuum limit of QCD.

The present calculations were performed predominantly with the coarse MILC lattices with a lattice spacing of  $b \sim 0.125$  fm, and a spatial extent of  $L \sim 2.5$  fm. On these configurations, the strange quark was held fixed near its physical value while the degenerate light quarks were varied over a range of masses corresponding to the pion masses shown in Table II. See Ref. [31] for further details. Results were also obtained on a coarse MILC ensemble with a spatial extent of  $L \sim 3.5$  fm. However, this data is

statistics limited. In addition, calculations were performed on two fine MILC ensembles at  $L \sim 2.5$  fm with  $b \sim 0.09$  fm. On the coarse MILC lattices, Dirichlet boundary conditions were implemented to reduce the original time extent of 64 down to 32, which saved a nominal factor of 2 in computational time. While this procedure leads to minimal degradation of a nucleon signal, it does limit the number of time slices available for fitting meson properties. By contrast, on the fine MILC ensembles, antiperiodic boundary conditions were implemented and all time slices are available.

The correlation function that projects onto the zero momentum state for the meson-baryon system is

$$C_{\phi B}(t) = \mathcal{P}_{ij} \sum_{\mathbf{x}, \mathbf{y}} \langle \phi^\dagger(t, \mathbf{x}) \bar{B}_i(t, \mathbf{y}) \phi(0, \mathbf{0}) B_j(0, \mathbf{0}) \rangle, \quad (13)$$

where  $\mathcal{P}_{ij}$  is a positive-energy projector. For instance, in the case of  $K^+ p$ , the interpolating operators for the  $K^+$  and the proton are

$$\phi(t, \mathbf{x}) = K^+(t, \mathbf{x}) = \bar{s}(t, \mathbf{x}) \gamma_5 u(t, \mathbf{x});$$

$$B_i(t, \mathbf{x}) = p_i(t, \mathbf{x}) = \epsilon_{abc} u_i^a(t, \mathbf{x}) (u^{bT}(t, \mathbf{x}) C \gamma_5 d^c(t, \mathbf{x})). \quad (14)$$

The masses of the mesons and baryons are extracted using the assumed form of the large-time behavior of the single-particle correlators as a function of time. As  $t \rightarrow \infty$ , the ground state dominates; however, fluctuations of the correlator increase with respect to the ground state. The meson and baryon two-point correlators,  $C_\phi(t)$  and  $C_B(t)$ , behave as

$$C_\phi(t) \rightarrow \mathcal{A}_1 e^{-m_\phi t}, \quad C_B(t) \rightarrow \mathcal{A}_2 e^{-m_B t}, \quad (15)$$

respectively, in the limits  $t \rightarrow \infty$  and  $L \rightarrow \infty$ . In relatively large lattice volumes the energy difference between the interacting and noninteracting meson-baryon states is a small fraction of the total energy, which is dominated by

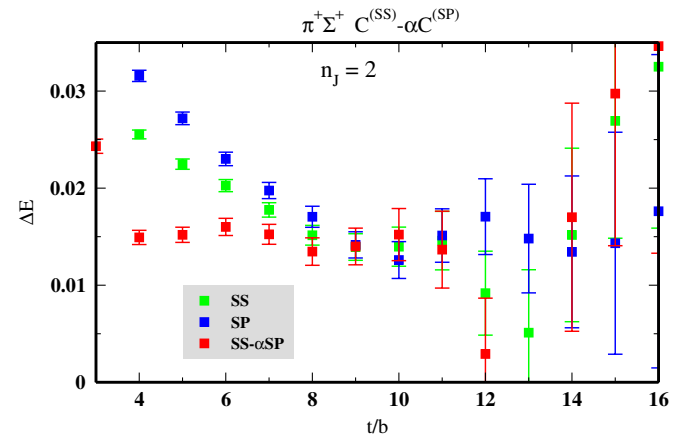


FIG. 1 (color online). Effective  $\Delta E_{\pi^+\Sigma^+}$  plot for coarse MILC ensemble (ii) from correlation functions  $C^{(SS)}$ ,  $C^{(SP)}$  and  $C^{(SS)} - \alpha C^{(SP)}$ . By taking the linear combination with  $\alpha$  tuned to remove the first excited state, earlier time slices are gained for fitting.

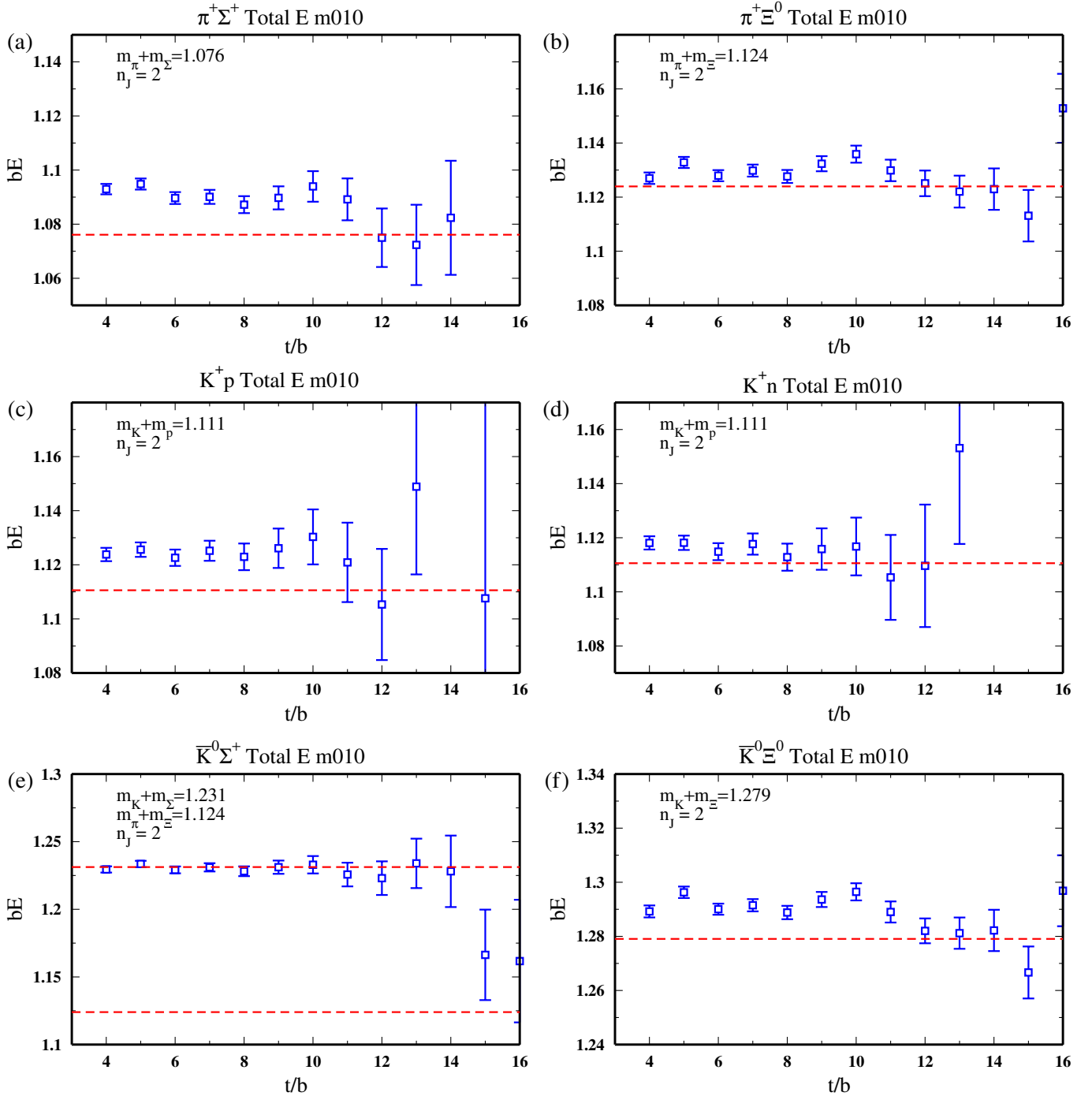


FIG. 2 (color online). Effective energy plots of the six meson-baryon processes shown in Table I. The plots are from MILC ensemble (ii),  $n_J = 2$ , and the linear combination  $C^{(SS)} - \alpha C^{(SP)}$  is plotted. The dashed line is the sum of the meson and baryon masses for each process, while the error bars represent the jackknife uncertainty. Note that the bE axis of (e) is a factor of 2 larger in span than the other plots to encompass the dashed line at  $m_\pi + m_\Xi = 1.124$ .

the masses of the mesons and baryons [1]. In order to extract this energy difference the ratio of correlation functions,  $G_{\phi B}(t)$ , is formed

$$G_{\phi B}(t) \equiv \frac{C_{\phi B}(t)}{C_\phi(t)C_B(t)} = \sum_{n=0}^{\infty} \mathcal{D}_n e^{-\Delta E_n t}, \quad (16)$$

where  $\Delta E \equiv \Delta E_0$  is the desired energy shift. With  $\Delta E$ , and the extracted masses of the meson and baryon, the scattering length can be calculated using Eqs. (7) and (9), or, if  $a \ll L$ , from Eq. (10). For the meson-baryon scattering lengths calculated in this work, the difference between the exact and perturbative eigen-equations is negligible.

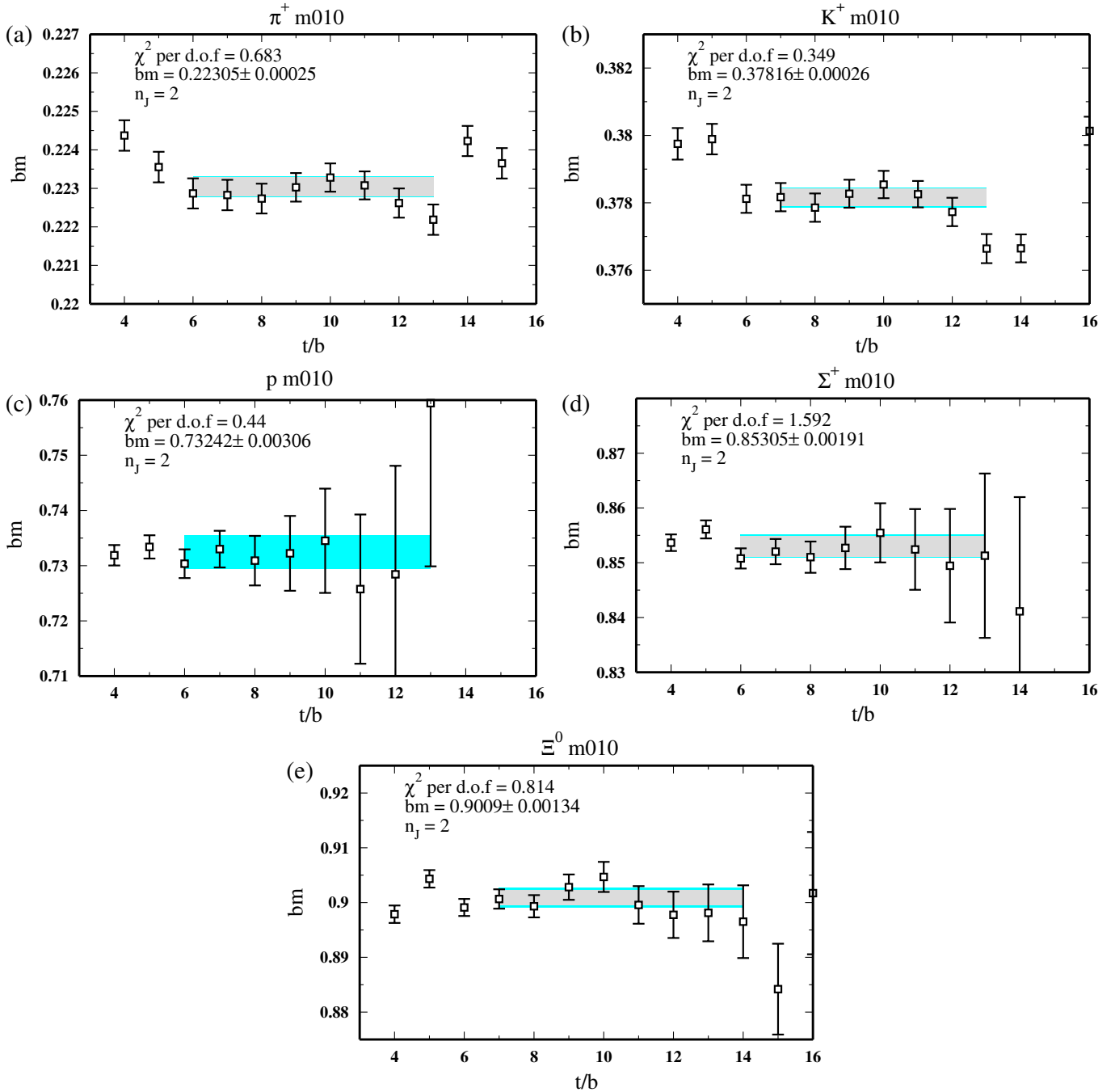


FIG. 3 (color online). Single-particle effective mass plots for coarse MILC ensemble (ii). Here we choose  $n_J = 2$ , and the linear combination  $C^{(SS)} - \alpha C^{(SP)}$  is plotted. The inner shaded bands are the jackknife uncertainties of the fits to the effective masses, and the outer bands are the jackknife uncertainty and systematic uncertainty added in quadrature over the indicated window of time slices.

A variety of fitting methods have been used, including standard chi-square minimization fits to one and two exponentials. Generalized effective energy plots are particularly useful for analyzing the lattice data and for estimating systematic errors [10]. These plots are constructed by taking the ratio of the correlators at times  $t$ , and  $t + n_J$  (where  $n_J$  is an integer)

$$\begin{aligned}
 m_{\phi,B}^{\text{eff}} &= \frac{1}{n_J} \log\left(\frac{C_{\phi,B}(t)}{C_{\phi,B}(t+n_J)}\right), \\
 \Delta E_{\phi,B}^{\text{eff}} &= \frac{1}{n_J} \log\left(\frac{G_{\phi,B}(t)}{G_{\phi,B}(t+n_J)}\right).
 \end{aligned}
 \tag{17}$$

With  $n_J = 1$ , the standard effective mass and energy plots

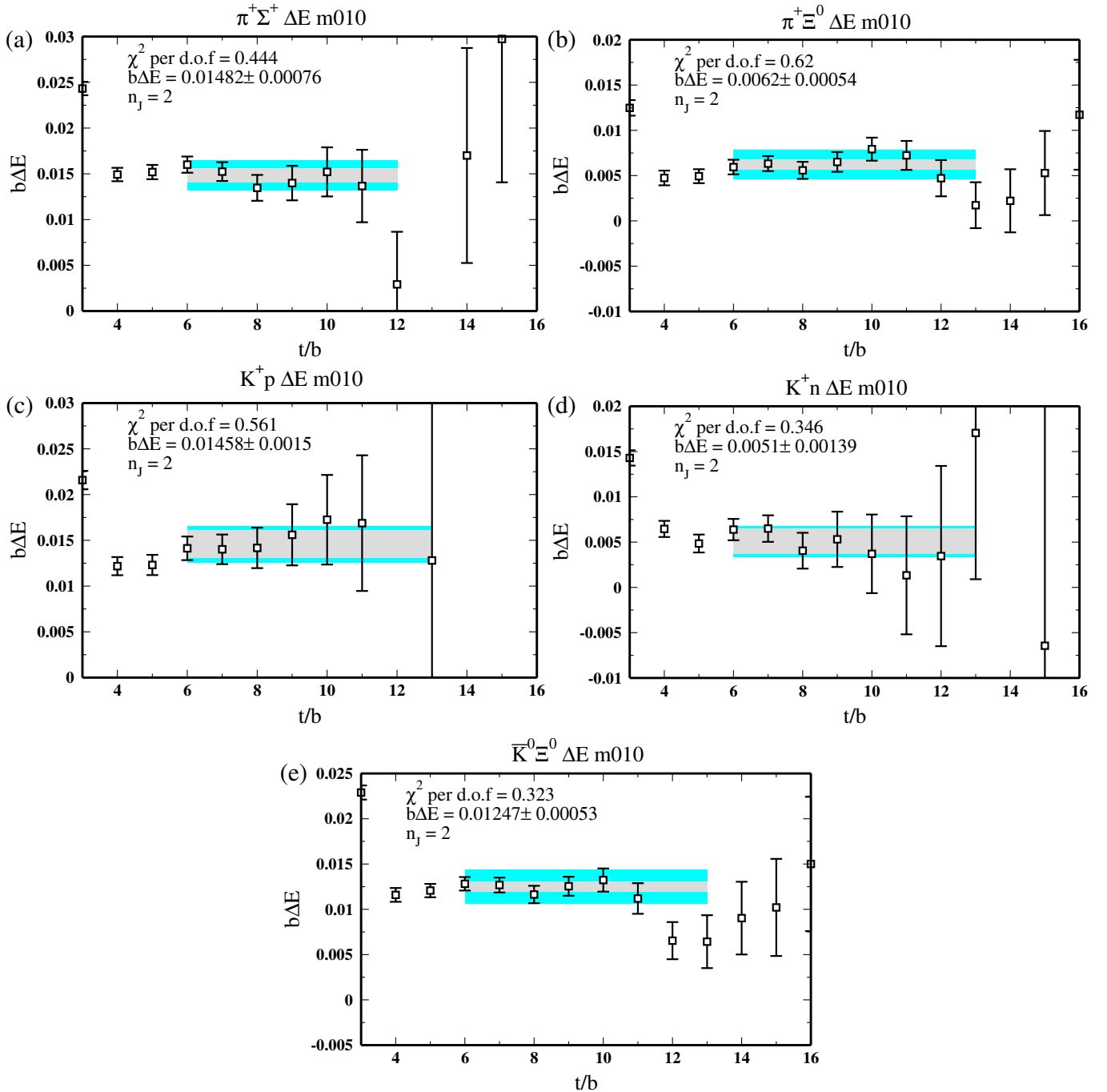


FIG. 4 (color online). Meson-baryon effective energy difference plots for coarse MILC ensemble (ii). Here we choose  $n_j = 2$ , and the linear combination  $C^{(SS)} - \alpha C^{(SP)}$  is plotted. The inner shaded bands are the jackknife uncertainties of the fits to the effective energy differences, and the outer bands are the jackknife uncertainty and systematic uncertainty added in quadrature over the indicated window of time slices.

are recovered. Generalized effective masses form a system of linear equations for each  $n_j$  over the time interval where the data is fit. For instance, if the interval is given by  $\Delta t = t_2 - t_1$ , then there is one equation for  $m^{\text{eff}}$  at each  $t$ , for any  $n_j$  that fits within  $\Delta t$ . The equations can be solved for  $m^{\text{eff}}$  by casting them into the form of the so-called normal equation [61]. Since each  $n_j$  constitutes a different effec-

tive mass plot, the number of degrees of freedom is increased significantly. This method provides a fitting routine that is faster than standard least-squares fitting. Additional details regarding the utility of generalized effective mass and energy plots can be found in Ref. [62].

The interpolating operator at the source is constructed from gauge-invariantly-smearred quark field operators,

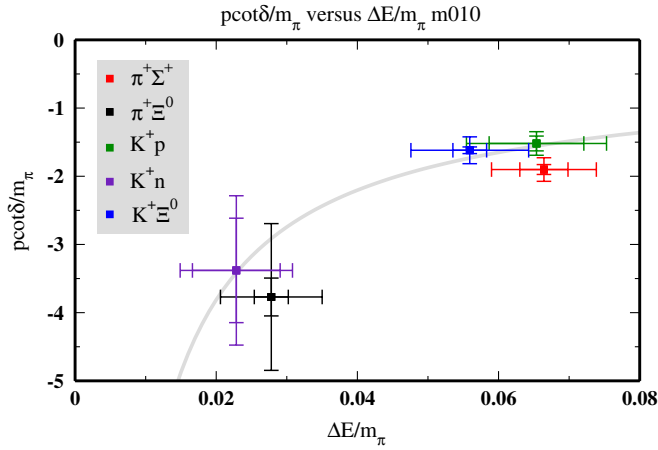


FIG. 5 (color online).  $p \cot \delta / m_\pi$  versus  $\Delta E_{\phi B} / m_\pi$  for the five elastic-scattering processes from coarse MILC ensemble (ii). The curve shown is  $p \cot \delta / m_\pi$  for the case of  $m_\phi = m_K$ , and  $m_B = m_p$ .

while at the sink, the interpolating operator is constructed from either local quark field operators, or from the same smeared quark field operators used at the source, leading to two sets of correlation functions. For brevity, we refer to the two sets of correlation functions that result from these source and sink operators as *smeared-point* (SP) and *smeared-smeared* (SS) correlation functions, respectively. By forming a linear combination of the SP and SS correlation functions,  $C^{(SS)} - \alpha C^{(SP)}$ , we are able to remove the first excited state, thus gaining early time slices for fitting [62]. This effect is illustrated in Fig. 1, which is the effective  $\Delta E_{\pi^+\Sigma^+}$  plot for coarse MILC ensemble (ii). We plot  $C^{(SS)}$ ,  $C^{(SP)}$ , and  $C^{(SS)} - \alpha C^{(SP)}$  with  $\alpha$  tuned to remove the first excited state. The effective energies, effective masses, and energy splittings are plotted for coarse MILC ensemble (ii) in Figs. 2–4. All of the necessary quantities needed for extraction of the scattering lengths are contained in Table III, which also contains the sum of meson and baryon masses at each quark mass. Figure 5

shows the results for all five processes, and the behavior of Eq. (7), versus the interaction energy, presented in terms of the dimensionless quantities  $p \cot \delta / m_\pi$  and  $\Delta E / m_\pi$ . The curve shown in Fig. 5 is  $p \cot \delta / m_\pi$  for the case of  $m_\phi = m_K$ , and  $m_B = m_p$ , as  $\Delta E / m_\pi$  is varied.  $S(\eta)$  in Eq. (8) is a function of the meson and baryon masses, so there will be a unique curve for each combination of  $m_\phi$  and  $m_B$ . Consequently, the  $K^+ p$ , and  $K^+ n$  data points fall on this curve.

## V. THE MIXED CHANNEL

As is clear from Table I, the  $\pi^+\Xi^0$  and  $\bar{K}^0\Sigma^+$  states carry the same global quantum numbers, and therefore couple to the same energy-eigenstates in the finite lattice volume. For energies above both kinematic thresholds, a determination of the three scattering parameters associated with these states (two phases and one mixing-angle) requires a coupled-channel analysis. Therefore, three energy levels above both kinematic thresholds must be determined in the lattice calculation to fully characterize scattering in this kinematic regime. In the present lattice volumes, the two-particle energies in these channels are close to the respective kinematic thresholds, and the energy of the lower-lying  $\pi^+\Xi^0$  state (which is below the  $\bar{K}^0\Sigma^+$  threshold) is determined by the low-energy elastic-scattering parameters, making it amenable to analysis using Eqs. (7)–(10).

*A priori*, one would expect both the  $\pi^+\Xi^0$  and  $\bar{K}^0\Sigma^+$  interpolating operators to couple to a common ground state (dominantly the  $\pi^+\Xi^0$  state), with a  $\bar{K}^0\Sigma^+$ -related level as the first excited state (for the lattice volumes considered here, the noninteracting  $\pi^+\Xi^0$  system with two units of relative momentum has an energy considerably above the  $\bar{K}^0\Sigma^+$  threshold). Interestingly, within our statistical and systematic uncertainties, we find distinct energy levels from the two interpolating operators. This is consistent with strong coupling to the color-singlet constituents of the interpolating operator and only very weak couplings to

TABLE II. The parameters of the MILC gauge configurations and domain-wall propagators used in this work. The subscript  $l$  denotes light quark (up and down), and  $s$  denotes the strange quark. The superscript  $dwf$  denotes the bare-quark mass for the domain-wall fermion propagator calculation. The last column is the number of configurations times the number of sources per configuration. Ensembles (i)–(iv) have  $L \sim 2.5$  fm and  $b \sim 0.125$  fm; Ensemble (v) has  $L \sim 3.5$  fm and  $b \sim 0.125$  fm; Ensembles (vi), (vii) have  $L \sim 2.5$  fm and  $b \sim 0.09$  fm.

Ensemble	$m_\pi$ (MeV)	$bm_l$	$bm_s$	$bm_l^{dwf}$	$bm_s^{dwf}$	$10^3 \times bm_{\text{res}}^a$	# of props
(i) 2064f21b676m007m050	291	0.007	0.050	0.0081	0.081	$1.604 \pm 0.038$	$1039 \times 24$
(ii) 2064f21b676m010m050	352	0.010	0.050	0.0138	0.081	$1.552 \pm 0.027$	$769 \times 24$
(iii) 2064f21b679m020m050	491	0.020	0.050	0.0313	0.081	$1.239 \pm 0.028$	$486 \times 24$
(iv) 2064f21b681m030m050	591	0.030	0.050	0.0478	0.081	$0.982 \pm 0.030$	$564 \times 24$
(v) 2864f21b676m010m050	352	0.010	0.050	0.0138	0.081	$1.552 \pm 0.027$	$128 \times 8$
(vi) 2896f21b709m0062m031	320	0.0062	0.031	0.0080	0.0423	$0.380 \pm 0.006$	$1001 \times 8$
(vii) 2896f21b709m0124m031	441	0.0124	0.031	0.0080	0.0423	$0.380 \pm 0.006$	$513 \times 3$

<sup>a</sup>Computed by the LHP collaboration for the coarse ensembles.

TABLE III. Lattice calculation results from the four coarse MILC ensembles which enter the analysis of the meson-baryon scattering lengths. The first uncertainty is statistical and the second uncertainty is systematic due to fitting. All quantities are in lattice units.

Quantity	m007 (i)	m010 (ii)	m020 (iii)	m030 (iv)
$m_\pi$	0.18384(31)(03)	0.22305(25)(08)	0.31031(38)(95)	0.37513(44)(13)
$m_K$	0.36783(32)(42)	0.37816(26)(11)	0.40510(33)(37)	0.43091(66)(16)
$m_p$	0.6978(61)(08)	0.7324(31)(10)	0.8069(22)(14)	0.8741(16)(05)
$m_\Sigma$	0.8390(22)(03)	0.8531(19)(08)	0.8830(18)(17)	0.9213(13)(03)
$m_\Xi$	0.8872(13)(16)	0.9009(13)(10)	0.9233(18)(04)	0.9461(14)(08)
$f_\pi$	0.09257(16)	0.09600(14)	0.10208(14)	0.10763(32)
$f_K$	0.10734(10)	0.10781(18)	0.10976(17)	0.11253(31)
$\Delta E_{\pi\Sigma}$	0.0150(14)(08)	0.0148(08)(13)	0.0111(10)(08)	0.0100(10)(11)
$\Delta E_{\pi\Xi}$	0.00646(64)(98)	0.0062(05)(12)	0.00431(68)(43)	0.00421(76)(60)
$\Delta E_{Kp}$	0.0140(22)(30)	0.0146(15)(13)	0.0092(10)(51)	0.0087(16)(16)
$\Delta E_{Kn}$	0.0057(18)(16)	0.0051(14)(09)	0.0036(09)(12)	0.0028(10)(11)
$\Delta E_{K\Xi}$	0.0118(08)(13)	0.0125(05)(14)	0.0085(08)(31)	0.0086(16)(16)
$a_{\pi\Sigma}$	-2.12(16)(09)	-2.36(09)(15)	-2.30(15)(13)	-2.36(18)(19)
$a_{\pi\Xi}$	-1.08(09)(14)	-1.19(09)(20)	-1.08(15)(09)	-1.20(18)(15)
$a_{Kp}$	-2.80(32)(44)	-2.95(21)(19)	-2.3(0.2)(1.0)	-2.27(31)(32)
$a_{Kn}$	-1.41(37)(34)	-1.33(30)(21)	-1.05(22)(30)	-0.89(27)(31)
$a_{K\Xi}$	-2.62(13)(21)	-2.77(08)(23)	-2.18(15)(63)	-2.29(30)(32)
$m_\pi + m_p$	0.8817(61)	0.9555(31)	1.1172(23)	1.2492(18)
$m_\pi + m_\Sigma$	1.0229(23)	1.0761(20)	1.1933(19)	1.2964(15)
$m_\pi + m_\Xi$	1.0710(14)	1.1240(14)	1.2336(19)	1.3212(16)
$m_K + m_p$	1.0657(61)	1.1106(31)	1.2119(23)	1.3050(19)
$m_K + m_\Sigma$	1.2069(23)	1.2312(20)	1.2881(19)	1.3522(16)
$m_K + m_\Xi$	1.2550(14)	1.2791(15)	1.3284(19)	1.3770(17)

states that require color rearrangement (see Fig. 2). While this is suggestive that mixing between the states is small, a definitive interpretation requires an extraction of three energy levels above the kinematic thresholds of the  $\pi^+\Xi^0$  and  $\bar{K}^0\Sigma^+$ , and below the next kinematic threshold, in order to determine the three scattering parameters. The optimal way to extract these levels is to use the variational method [63,64], which requires the full matrix of correlation functions to be calculated, and diagonalized. The extraction of the scattering parameters would then proceed via an extension of the variational method to the coupled-channel scenario [65,66].

Because of our incomplete knowledge of the three mixed-channel energy levels, we do not attempt to extract any  $\bar{K}^0\Sigma^+$  scattering parameters in this work.

## VI. $SU(3)$ HB $\chi$ PT EXTRAPOLATION

### A. Scattering length formulas

The scattering lengths of the five meson-baryon processes listed in Eq. (5) are, to  $\mathcal{O}(m_\pi^3)$  in  $SU(3)$  HB $\chi$ -PT [15,16],

$$a_{\pi^+\Sigma^+} = \frac{1}{4\pi} \frac{m_\Sigma}{m_\pi + m_\Sigma} \left[ -\frac{2m_\pi}{f_\pi^2} + \frac{2m_\pi^2}{f_\pi^2} C_1 + \mathcal{Y}_{\pi^+\Sigma^+}(\mu) + 8h_{123}(\mu) \frac{m_\pi^3}{f_\pi^2} \right]; \quad (18)$$

$$a_{\pi^+\Xi^0} = \frac{1}{4\pi} \frac{m_\Xi}{m_\pi + m_\Xi} \left[ -\frac{m_\pi}{f_\pi^2} + \frac{m_\pi^2}{f_\pi^2} C_{01} + \mathcal{Y}_{\pi^+\Xi^0}(\mu) + 8h_1(\mu) \frac{m_\pi^3}{f_\pi^2} \right]; \quad (19)$$

$$a_{K^+p} = \frac{1}{4\pi} \frac{m_N}{m_K + m_N} \left[ -\frac{2m_K}{f_K^2} + \frac{2m_K^2}{f_K^2} C_1 + \mathcal{Y}_{K^+p}(\mu) + 8h_{123}(\mu) \frac{m_K^3}{f_K^2} \right]; \quad (20)$$

$$a_{K^+n} = \frac{1}{4\pi} \frac{m_N}{m_K + m_N} \left[ -\frac{m_K}{f_K^2} + \frac{m_K^2}{f_K^2} C_{01} + \mathcal{Y}_{K^+n}(\mu) + 8h_1(\mu) \frac{m_K^3}{f_K^2} \right]; \quad (21)$$

$$a_{\bar{K}^0\Xi^0} = \frac{1}{4\pi} \frac{m_\Xi}{m_K + m_\Xi} \left[ -\frac{2m_K}{f_K^2} + \frac{2m_K^2}{f_K^2} C_1 + \mathcal{Y}_{\bar{K}^0\Xi^0}(\mu) + 8h_{123}(\mu) \frac{m_K^3}{f_K^2} \right]; \quad (22)$$

where we have defined  $C_{01} \equiv C_0 + C_1$  and  $h_{123} \equiv h_1 - h_2 + h_3$ , and the loop functions are given by

$$\begin{aligned} \mathcal{Y}_{\pi^+\Sigma^+}(\mu) &= \frac{m_\pi^2}{2\pi^2 f_\pi^4} \left\{ -m_\pi \left( \frac{3}{2} - 2 \ln \frac{m_\pi}{\mu} - \ln \frac{m_K}{\mu} \right) \right. \\ &\quad \left. - \sqrt{m_K^2 - m_\pi^2} \arccos \frac{m_\pi}{m_K} \right. \\ &\quad \left. + \frac{\pi}{2} \left[ 3F^2 m_\pi - \frac{1}{3} D^2 m_\eta \right] \right\}; \end{aligned} \quad (23)$$

$$\begin{aligned} \mathcal{Y}_{\pi^+\Xi^0}(\mu) &= \frac{m_\pi^2}{4\pi^2 f_\pi^4} \left\{ -m_\pi \left( \frac{3}{2} - 2 \ln \frac{m_\pi}{\mu} - \ln \frac{m_K}{\mu} \right) \right. \\ &\quad \left. - \sqrt{m_K^2 - m_\pi^2} \left( \pi + \arccos \frac{m_\pi}{m_K} \right) \right. \\ &\quad \left. + \frac{\pi}{4} \left[ 3(D-F)^2 m_\pi - \frac{1}{3} (D+3F)^2 m_\eta \right] \right\}; \end{aligned} \quad (24)$$

$$\begin{aligned} \mathcal{Y}_{K^+p}(\mu) &= \frac{m_K^2}{4\pi^2 f_K^4} \left\{ m_K \left( -3 + 2 \ln \frac{m_\pi}{\mu} + \ln \frac{m_K}{\mu} + 3 \ln \frac{m_\eta}{\mu} \right) \right. \\ &\quad \left. + 2\sqrt{m_K^2 - m_\pi^2} \ln \frac{m_K + \sqrt{m_K^2 - m_\pi^2}}{m_\pi} \right. \\ &\quad \left. - 3\sqrt{m_\eta^2 - m_K^2} \arccos \frac{m_K}{m_\eta} - \frac{\pi}{6} (D-3F) \right. \\ &\quad \left. \times \left[ 2(D+F) \frac{m_\pi^2}{m_\eta + m_\pi} + (D+5F)m_\eta \right] \right\}; \end{aligned} \quad (25)$$

$$\begin{aligned} \mathcal{Y}_{K^+n}(\mu) &= \frac{\mathcal{Y}_{K^+p}}{2} + \frac{3m_K^2}{8\pi^2 f_K^4} \left\{ m_K \left( \ln \frac{m_\pi}{\mu} - \ln \frac{m_K}{\mu} \right) \right. \\ &\quad \left. + \sqrt{m_K^2 - m_\pi^2} \ln \frac{m_K + \sqrt{m_K^2 - m_\pi^2}}{m_\pi} \right. \\ &\quad \left. + \frac{\pi}{3} (D-3F) \left[ (D+F) \frac{m_\pi^2}{m_\eta + m_\pi} \right. \right. \\ &\quad \left. \left. + \frac{1}{6} (7D+3F)m_\eta \right] \right\}; \end{aligned} \quad (26)$$

$$\begin{aligned} \mathcal{Y}_{\bar{K}^0\Xi^0}^{(1)}(\mu) &= \frac{m_K^2}{4\pi^2 f_K^4} \left\{ m_K \left( -3 + 2 \ln \frac{m_\pi}{\mu} + \ln \frac{m_K}{\mu} + 3 \ln \frac{m_\eta}{\mu} \right) \right. \\ &\quad \left. + 2\sqrt{m_K^2 - m_\pi^2} \ln \frac{m_K + \sqrt{m_K^2 - m_\pi^2}}{m_\pi} \right. \\ &\quad \left. - 3\sqrt{m_\eta^2 - m_K^2} \arccos \frac{m_K}{m_\eta} - \frac{\pi}{6} (D+3F) \right. \\ &\quad \left. \times \left[ 2(D-F) \frac{m_\pi^2}{m_\eta + m_\pi} + (D-5F)m_\eta \right] \right\}. \end{aligned} \quad (27)$$

In what follows, we choose  $\mu = \Lambda_\chi = 4\pi f_\pi$  and evaluate

$f_\pi$  at its lattice physical value [42], and we take  $m_\eta$  from the Gell-Mann-Okubo formula. These choices modify the chiral expansion at  $\mathcal{O}(m_\pi^4)$  and are therefore consistent to the order we are working. The first mixed-action modification to these HB $\chi$ -PT extrapolation formulas appear as corrections to these loop functions,  $\mathcal{Y}_{\phi B}$ , and to the corresponding counterterms which absorb the scale dependence. Some of the mesons propagating in the loops appear as mixed valence-sea combinations, and thus the corresponding meson masses appearing in these functions are heavier by a known amount [67]. The precise form of the predicted corrections require a computation of the scattering processes with mixed-action/partially quenched  $\chi$ -PT.

Our physical parameters are consistent with Ref. [18] (note that our decay constant convention differs by  $\sqrt{2}$ ). Namely,  $f_\pi = 130.7$  MeV,  $m_\pi = 139.57$  MeV,  $f_K = 159.8$  MeV,  $m_K = 493.68$  MeV,  $m_N = 938$  MeV,  $m_\Sigma = 1192$  MeV and  $m_\Xi = 1314$  MeV. The axial couplings,  $D$  and  $F$ , for coarse MILC ensembles (ii)–(iv) are taken from the mixed-action calculation of Ref. [68], and we extrapolate for coarse MILC ensemble (i) using these values.

## B. Extrapolation to the physical point

For the purposes of fitting and visualization, it is useful to construct from the scattering lengths the functions  $\Gamma^{(1,2)}$  which are polynomials in  $m_\phi$ . For the  $\pi^+\Sigma^+$ ,  $K^+p$ , and  $\bar{K}^0\Xi^0$  processes one defines<sup>5</sup>

$$\Gamma_{\text{LO}}^{(1)} \equiv -\frac{2\pi a f_\phi^2}{m_\phi} \left( 1 + \frac{m_\phi}{m_B} \right) = 1; \quad (28)$$

$$\Gamma_{\text{NLO}}^{(1)} \equiv -\frac{2\pi a f_\phi^2}{m_\phi} \left( 1 + \frac{m_\phi}{m_B} \right) = 1 - C_1 m_\phi; \quad (29)$$

$$\begin{aligned} \Gamma_{\text{NNLO}}^{(1)} &\equiv -\frac{2\pi a f_\phi^2}{m_\phi} \left( 1 + \frac{m_\phi}{m_B} \right) + \frac{f_\phi^2}{2m_\phi} \mathcal{Y}_{\phi B}(\Lambda_\chi) \\ &= 1 - C_1 m_\phi - 4h_{123}(\Lambda_\chi) m_\phi^2, \end{aligned} \quad (30)$$

and for the  $\pi^+\Xi^0$ , and  $K^+n$  processes one defines

$$\Gamma_{\text{LO}}^{(2)} \equiv -\frac{4\pi a f_\phi^2}{m_\phi} \left( 1 + \frac{m_\phi}{m_B} \right) = 1; \quad (31)$$

$$\Gamma_{\text{NLO}}^{(2)} \equiv -\frac{4\pi a f_\phi^2}{m_\phi} \left( 1 + \frac{m_\phi}{m_B} \right) = 1 - C_{01} m_\phi; \quad (32)$$

$$\begin{aligned} \Gamma_{\text{NNLO}}^{(2)} &\equiv -\frac{4\pi a f_\phi^2}{m_\phi} \left( 1 + \frac{m_\phi}{m_B} \right) + \frac{f_\phi^2}{m_\phi} \mathcal{Y}_{\phi B}(\Lambda_\chi) \\ &= 1 - C_{01} m_\phi - 8h_1(\Lambda_\chi) m_\phi^2. \end{aligned} \quad (33)$$

<sup>5</sup>Here we use the standard notation, LO = leading order, NLO = next-to-leading order and so on.

Notice that the left-hand sides of these equations are given entirely in terms of lattice-determined quantities, all evaluated under Jackknife, whereas the right-hand side provides a convenient polynomial fitting function. Plots of  $\Gamma_{\text{NLO}}$  formed from the lattice data (all ensembles listed in Table II) versus the Goldstone masses are given in Fig. 6. We see evidence in this plot that the fine and large-volume coarse data are statistically limited as compared to the

coarse data. Therefore, we include only the coarse data in our fits. The fine data is, however, indicative that lattice-spacing effects are small.

In the three-flavor chiral expansion, we have an over-determined system at both NLO and NNLO. While there are five observables, there are two low energy constants (LECs) at NLO,  $C_0$  and  $C_{01}$ , and two LECs at NNLO,  $h_1$  and  $h_{123}$ . Fits of the LECs from each process at NLO are

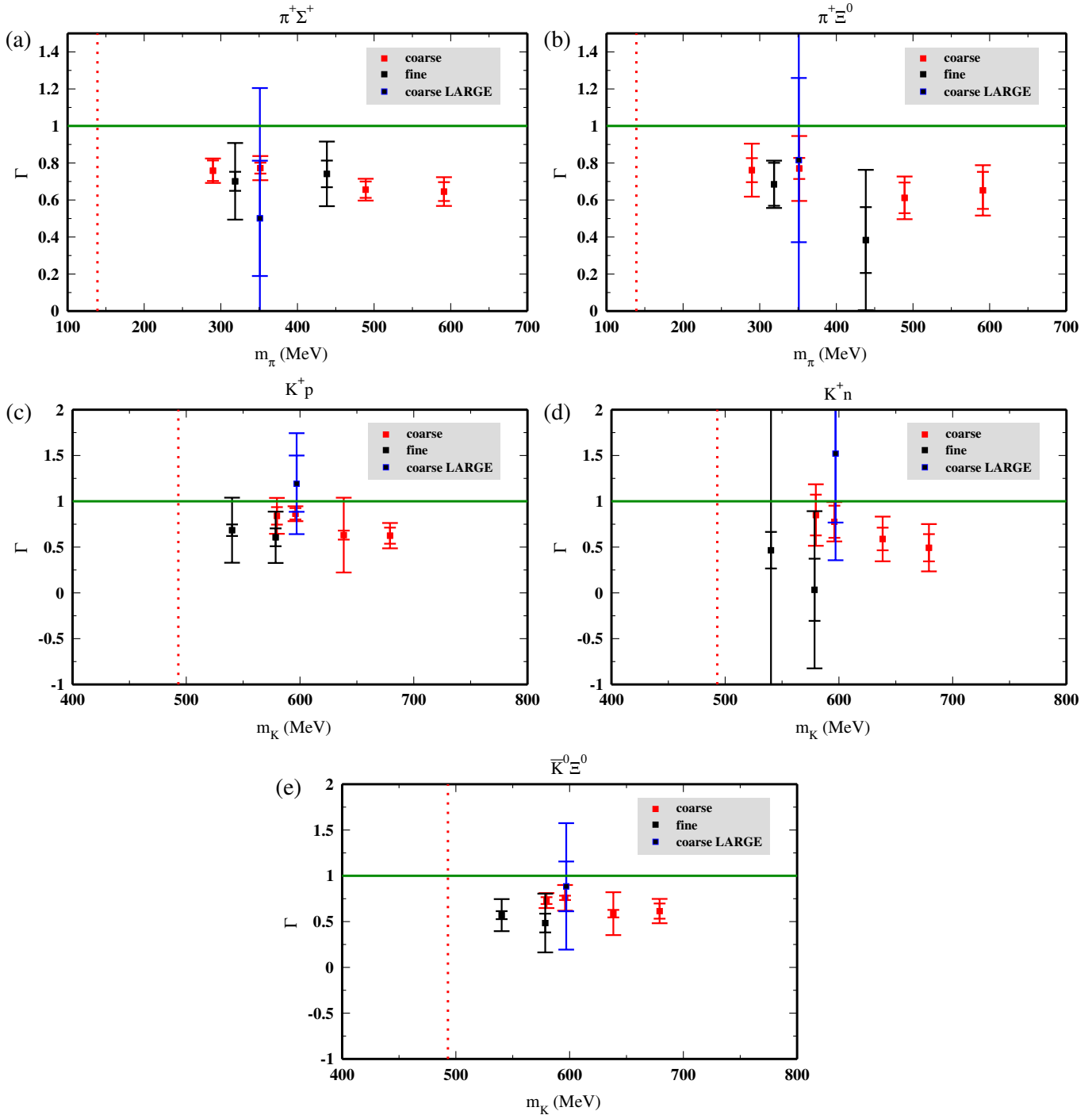


FIG. 6 (color online). Plots of  $\Gamma_{\text{NLO}}$  versus the Goldstone masses for the five meson-baryon processes. All lattice data is included.

TABLE IV.  $SU(3)$  LECs fit from each process at NLO, and from  $\pi^+\Sigma^+$ , and  $\pi^+\Xi^0$  at NNLO. The first uncertainty in parentheses is statistical, and the second is the statistical and systematic uncertainty added in quadrature.

Quantity	NLO fit each process	NNLO fit $\pi^+\Sigma^+$ , $\pi^+\Xi^0$
$C_1(\pi^+\Sigma^+)$	0.66(04)(11) GeV <sup>-1</sup>	3.51(18)(25) GeV <sup>-1</sup>
$C_{01}(\pi^+\Xi^0)$	0.69(06)(22) GeV <sup>-1</sup>	7.44(29)(69) GeV <sup>-1</sup>
$C_1(K^+p)$	0.44(09)(23) GeV <sup>-1</sup>	-
$C_{01}(K^+n)$	0.56(11)(27) GeV <sup>-1</sup>	-
$C_1(\bar{K}^0\Xi^0)$	0.50(06)(14) GeV <sup>-1</sup>	-
$h_1$	-	-0.59(08)(14) GeV <sup>-2</sup>
$h_{123}$	-	-0.42(10)(10) GeV <sup>-2</sup>

given in Table IV and the corresponding values of the scattering lengths are given in Table V. At NLO, the LECs are of natural size, and provide a consistent extraction within uncertainties. Correspondingly, the scattering lengths appear to deviate perturbatively from the LO values. The perturbative behavior of the scattering lengths at NLO is evident from the plots of  $\Gamma_{\text{NLO}}$  versus the Goldstone masses given in Fig. 7. Clearly the deviations of the lattice data from unity are consistent with a perturbative expansion.

At NNLO the situation changes dramatically. This is clear from the plots of  $\Gamma_{\text{NNLO}}$  versus the Goldstone masses given in Fig. 7. The shift of the value of  $\Gamma$  from NLO to NNLO is dependent on the renormalization scale  $\mu$ . With the choice  $\mu = \Lambda_\chi$  one would expect this shift to be perturbative. However, this is not the case and therefore loop corrections are very large at the scale  $\Lambda_\chi$ . There are many strategies that one may take to fit the LECs in the overdetermined system. Here we fit the LECs to the  $\pi^+\Sigma^+$  and  $\pi^+\Xi^0$  data, and then use these LECs to predict the kaon processes. Therefore, in Fig. 7, only (a) and (b) are fits. The fit LECs are given in Table IV. While the NNLO LECs  $h_1$  and  $h_{123}$  appear to be of natural size, the NLO LECs  $C_0$  and  $C_{01}$  are unnaturally large and therefore are countering the large loop effects. The extrapolated  $\pi^+\Sigma^+$  and  $\pi^+\Xi^0$  scattering lengths are given in Table V and appear to be perturbative. Table V also gives the extrapolated kaon-baryon scattering lengths with the LECs determined from the  $\pi^+\Sigma^+$  and  $\pi^+\Xi^0$  data. The resulting

NNLO predictions deviate by at least 100% from the LO values. Other fitting strategies lead to this same conclusion: the kaon-baryon scattering lengths are unstable against chiral corrections in the three-flavor chiral expansion, over the range of light-quark masses that we consider.

## VII. $SU(2)$ HB $\chi$ PT EXTRAPOLATION

Given the poor convergence seen in the three-flavor chiral expansion due to the large loop corrections, it is natural to consider the two-flavor theory with the strange quark integrated out. In this way,  $\pi\Sigma$  and  $\pi\Xi$  may be analyzed in an expansion in  $m_\pi$  with no fear of corrections that scale as powers of  $m_K$ . The detailed matching of LECs between the three- and two-flavor theories is described in detail in Ref. [18]. We make use of the formulation of the  $\pi\Sigma$  and  $\pi\Xi$   $T$ -matrices from [18] to perform the two-flavor chiral extrapolations for  $a_{\pi^+\Sigma^+}$ , and  $a_{\pi^+\Xi^0}$ . As pointed out in Ref. [18], there are two representations of the pion-hyperon scattering lengths that are equivalent up to omitted higher orders in the chiral expansion; one contains a chiral logarithm, and the other is purely a polynomial in  $m_\pi$ . Using both forms provides a useful check on the systematics of the chiral extrapolation.

### A. Scattering length formulas I

To  $\mathcal{O}(m_\pi^3)$  in the two-flavor chiral expansion,  $a_{\pi^+\Sigma^+}$  and  $a_{\pi^+\Xi^0}$  are given by [18]

$$a_{\pi^+\Sigma^+} = \frac{1}{4\pi} \frac{m_\Sigma}{m_\pi + m_\Sigma} \left[ -\frac{2m_\pi}{f_\pi^2} + \frac{2m_\pi^2}{f_\pi^2} C_{\pi^+\Sigma^+} + \frac{m_\pi^3}{\pi^2 f_\pi^4} \log \frac{m_\pi}{\mu} + \frac{2m_\pi^3}{f_\pi^2} h_{\pi^+\Sigma^+}(\mu) \right]; \quad (34)$$

$$a_{\pi^+\Xi^0} = \frac{1}{4\pi} \frac{m_\Xi}{m_\pi + m_\Xi} \left[ -\frac{m_\pi}{f_\pi^2} + \frac{m_\pi^2}{f_\pi^2} C_{\pi^+\Xi^0} + \frac{m_\pi^3}{2\pi^2 f_\pi^4} \log \frac{m_\pi}{\mu} + \frac{m_\pi^3}{f_\pi^2} h_{\pi^+\Xi^0}(\mu) \right], \quad (35)$$

where the explicit forms—in terms of Lagrangian parameters—of the LECs  $C_{\pi^+\Sigma^+}$ ,  $h_{\pi^+\Sigma^+}$ ,  $C_{\pi^+\Xi^0}$  and  $h_{\pi^+\Xi^0}$  are given in Ref. [18]. As in the three-flavor case, the mixed-action modification to the  $SU(2)$  scattering length formula

TABLE V.  $SU(3)$  extrapolated scattering lengths using the LECs from Table IV. The first uncertainty in parentheses is statistical, and the second is the statistical and systematic uncertainty added in quadrature. Note that the NLO (NNLO fit) column is using  $C_1$ ,  $C_{01}$  from the NNLO fit to  $\pi^+\Sigma^+$ ,  $\pi^+\Xi^0$ .

Quantity	LO (fm)	NLO fit (fm)	NLO (NNLO fit) (fm)	NNLO (fm)
$a_{\pi\Sigma}$	-0.2294	-0.208(01)(03)	-0.117(06)(08)	-0.197(06)(08)
$a_{\pi\Xi}$	-0.1158	-0.105(01)(04)	0.004(05)(11)	-0.096(05)(12)
$a_{Kp}$	-0.3971	-0.311(18)(44)	0.292(35)(48)	-0.154(51)(63)
$a_{Kn}$	-0.1986	-0.143(10)(27)	0.531(28)(68)	0.128(42)(87)
$a_{K\Xi}$	-0.4406	-0.331(12)(31)	0.324(39)(54)	-0.127(57)(70)

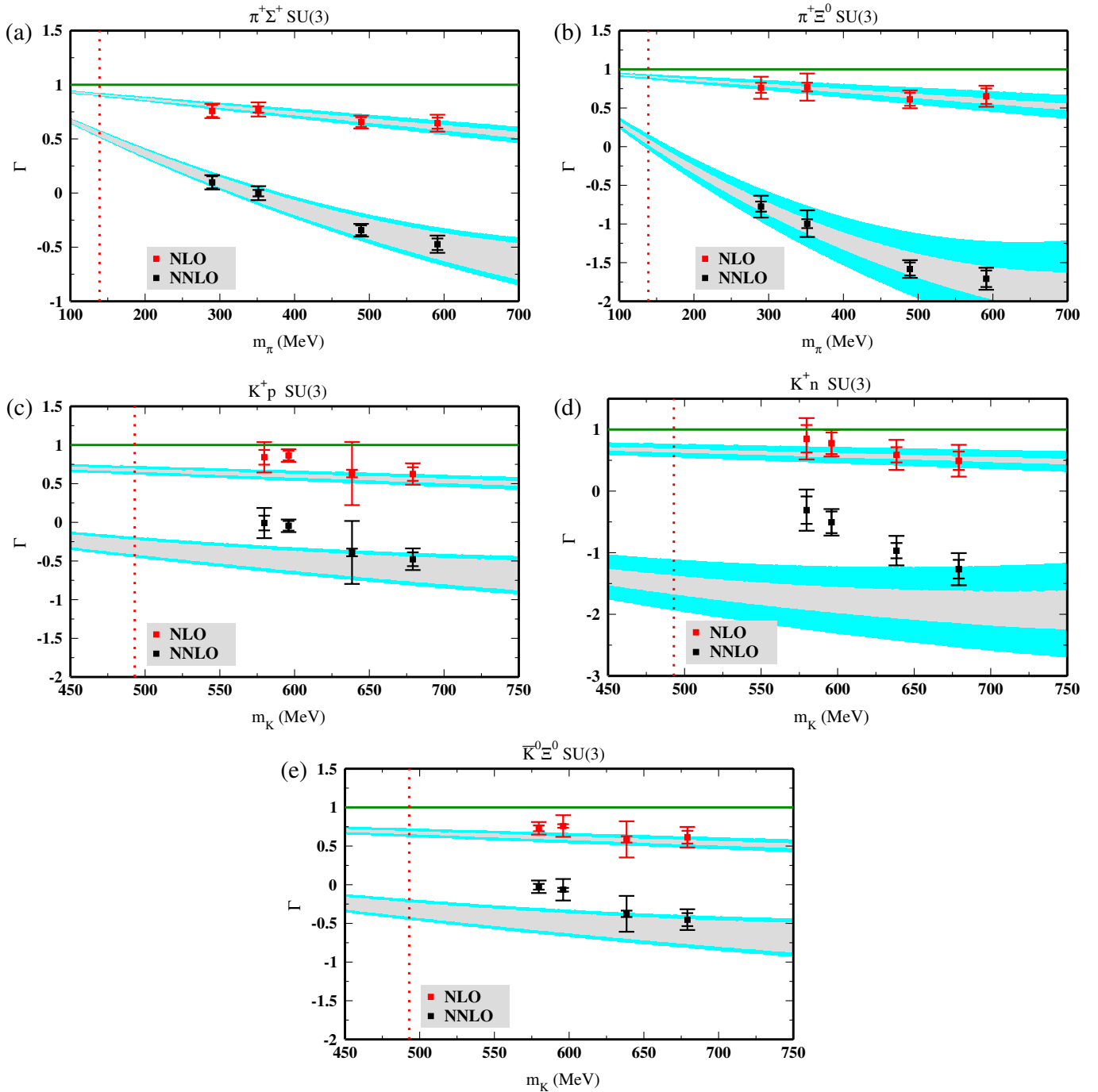


FIG. 7 (color online). Plots of  $\Gamma_{\text{NLO}}$  and  $\Gamma_{\text{NNLO}}$  versus the Goldstone masses. The line at  $\Gamma = 1$  is the leading order curve, and dotted line is the physical meson mass. The innermost error bar is the statistical uncertainty and the outermost error bar is the statistical and systematic uncertainty added in quadrature. The inner and outer filled bands correspond to the statistical and systematic uncertainty, respectively, of the fits to the LECs at NLO and NNLO using  $\pi^+\Sigma^+$ , and  $\pi^+\Xi^0$  only, for the  $SU(3)$  case.

would begin with corrections to the  $m_\pi^3 \ln(m_\pi)$  terms, with the mixed valence-sea pions having the known additive mass shift [67]. We again choose  $\mu = \Lambda_\chi = 4\pi f_\pi$  and evaluate  $f_\pi$  at its lattice physical value. In analogy with the three-flavor case, we define

$$\Gamma_{\text{LO}} \equiv 1; \quad (36)$$

$$\Gamma_{\text{NLO}} \equiv 1 - C_{\pi^+B} m_\pi; \quad (37)$$

$$\Gamma_{\text{NNLO}} \equiv 1 - C_{\pi^+B} m_\pi - h_{\pi^+B} (\Lambda_\chi) m_\pi^2, \quad (38)$$

where  $B$  is either  $\Sigma^+$  or  $\Xi^0$ . In Fig. 8 we give plots of  $\Gamma_{\text{NLO}}$  and  $\Gamma_{\text{NNLO}}$  versus the pion mass for the two-flavor case. Clearly the deviations of  $\Gamma$  from unity are consistent with a

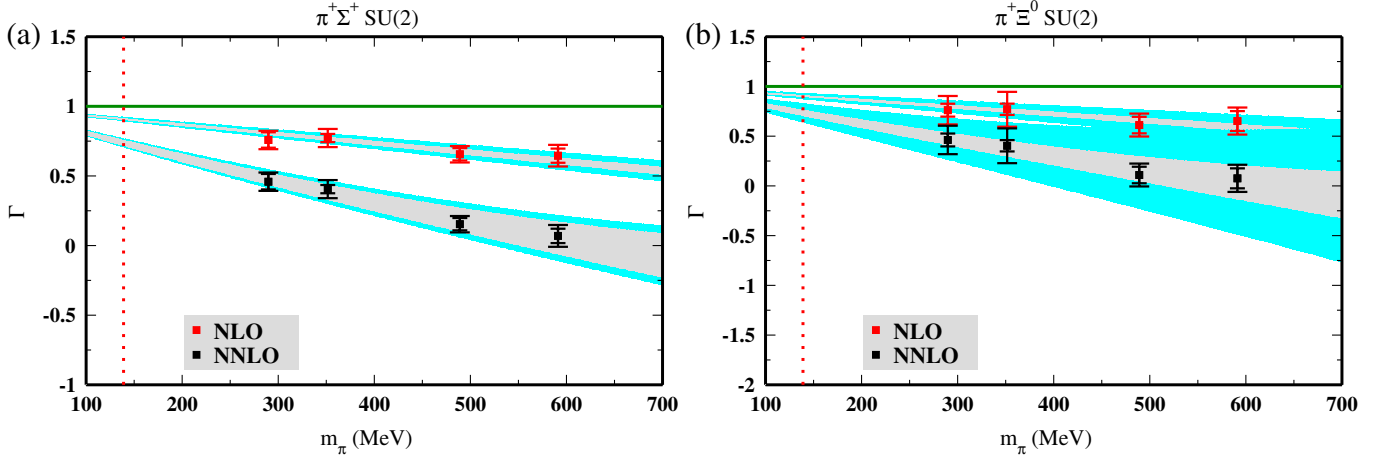


FIG. 8 (color online).  $\Gamma_{\text{NLO}}, \Gamma_{\text{NNLO}}$  plots for the  $\pi^+\Sigma^+$ , and  $\pi^+\Xi^0$  processes versus the pion mass. The line at  $\Gamma = 1$  is the leading order curve, and the dotted line is the physical pion mass. The innermost error bar is the statistical uncertainty and the outermost error bar is the statistical and systematic uncertainty added in quadrature. The inner and outer filled bands correspond to the statistical and systematic uncertainty, respectively, of the fits to the LECs at NLO and NNLO using  $\pi^+\Sigma^+$ , and  $\pi^+\Xi^0$  for the  $SU(2)$  case.

TABLE VI.  $SU(2)$  LECs fit from each process at NLO and at NNLO. The first uncertainty in parentheses is statistical, and the second is the statistical and systematic uncertainty added in quadrature.

	NLO fit	NNLO fit
$C_{\pi^+\Sigma^+}$	0.66(04)(11) $\text{GeV}^{-1}$	1.98(17)(24) $\text{GeV}^{-1}$
$C_{\pi^+\Xi^0}$	0.69(06)(22) $\text{GeV}^{-1}$	2.01(24)(68) $\text{GeV}^{-1}$
$h_{\pi^+\Sigma^+}$	-	-0.65(36)(40) $\text{GeV}^{-2}$
$h_{\pi^+\Xi^0}$	-	-0.6(0.5)(1.1) $\text{GeV}^{-2}$

perturbative expansion at both NLO and NNLO, showing that the loop corrections are much smaller at the scale  $\Lambda_\chi$  than in the three-flavor case. All extracted LECs are of natural size and given in Table VI. The extrapolated  $\pi^+\Sigma^+$  and  $\pi^+\Xi^0$  scattering lengths are given in Table VII. The results are consistent with what was found in the three-flavor extrapolation. The NLO and NNLO LECs are highly correlated in the NNLO fit. Figure 9 shows the 68% and 95% confidence interval error ellipses in the  $h$ - $C$  plane for

TABLE VII.  $SU(2)$  extrapolated scattering lengths using the LECs from Table VI. The first uncertainty in parentheses is statistical, and the second is the statistical and systematic uncertainty added in quadrature.

Quantity	LO (fm)	NLO (fm)	NLO (NNLO fit) (fm)	NNLO (fm)
$a_{\pi\Sigma}$	-0.2294	-0.208(01)(03)	-0.166(05)(08)	-0.197(06)(08)
$a_{\pi\Xi}$	-0.1158	-0.105(01)(04)	-0.083(04)(11)	-0.098(05)(12)

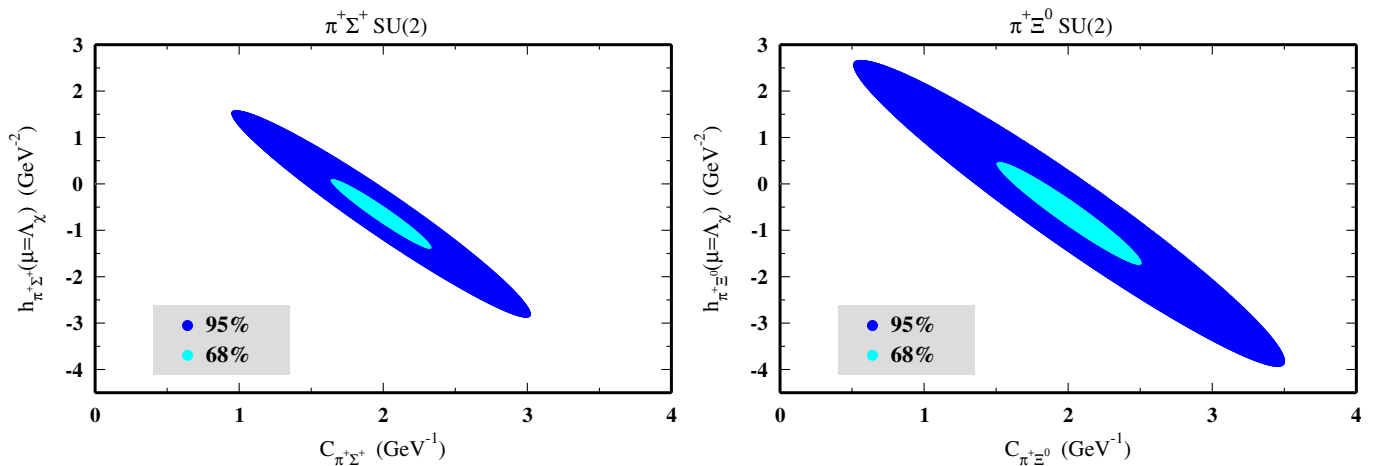


FIG. 9 (color online). The 68% (light) and 95% (dark) confidence interval error ellipses for fits for the  $\pi^+\Sigma^+$  (left), and  $\pi^+\Xi^0$  (right) processes using Eqs. (34) and (35).

TABLE VIII.  $SU(2)$  LECs fit from each process at NLO and at NNLO. The first uncertainty in parentheses is statistical, and the second is the statistical and systematic uncertainty added in quadrature.

	NLO fit	NNLO fit
$C_{\pi^+\Sigma^+}$	1.28(09)(11) GeV <sup>-1</sup>	1.90(10)(17) GeV <sup>-1</sup>
$C_{\pi^+\Xi^0}$	1.84(23)(25) GeV <sup>-1</sup>	1.93(12)(48) GeV <sup>-1</sup>
$h'_{\pi^+\Sigma^+}$	-	-1.33(21)(26) GeV <sup>-2</sup>
$h'_{\pi^+\Xi^0}$	-	-1.36(27)(75) GeV <sup>-2</sup>

both  $\pi^+\Sigma^+$  and  $\pi^+\Xi^0$ . Exploring the full 95% confidence interval error ellipse in the  $h$ - $C$  plane yields

$$a_{\pi^+\Sigma^+} = -0.197 \pm 0.017 \text{ fm}; \quad (39)$$

$$a_{\pi^+\Xi^0} = -0.098 \pm 0.017 \text{ fm}. \quad (40)$$

These are the numbers that we quote as our best determinations of the pion-hyperon scattering lengths.

### B. Scattering length formulas II

Reference [18] makes the interesting observation that replacing  $f_\pi$  with its chiral limit value,  $f$ , yields

$$a_{\pi^+\Sigma^+} = \frac{1}{2\pi} \frac{m_\Sigma}{m_\pi + m_\Sigma} \left[ -\frac{m_\pi}{f^2} + \frac{m_\pi^2}{f^2} C_{\pi^+\Sigma^+} + \frac{m_\pi^3}{f^2} h'_{\pi^+\Sigma^+} \right], \quad (41)$$

$$h'_{\pi^+\Sigma^+} = \frac{4}{f^2} \ell_4^r + h_{\pi^+\Sigma^+};$$

$$a_{\pi^+\Xi^0} = \frac{1}{4\pi} \frac{m_\Xi}{m_\pi + m_\Xi} \left[ -\frac{m_\pi}{f^2} + \frac{m_\pi^2}{f^2} C_{\pi^+\Xi^0} + \frac{m_\pi^3}{f^2} h'_{\pi^+\Xi^0} \right], \quad (42)$$

$$h'_{\pi^+\Xi^0} = \frac{4}{f^2} \ell_4^r + h_{\pi^+\Xi^0},$$

where  $\ell_4^r$  is the LEC which governs the pion mass dependence of  $f_\pi$  [69]. Note that the chiral logs have canceled, and in this form, valid to order  $m_\pi^3$  in the chiral expansion, the scattering lengths have a simple polynomial dependence on  $m_\pi$ . Taking the standard value  $f = 122.9$  MeV [18,69] and refitting the LECs yields the results tabulated in Table VIII. The extrapolated  $\pi^+\Sigma^+$  and  $\pi^+\Xi^0$  scattering lengths are given in Table IX. These results are clearly consistent with what was found in the two-flavor extrapolation with the chiral logarithm explicit. Figure 10 shows the 68% and 95% confidence interval error ellipses in the  $h$ - $C$  plane for both  $\pi^+\Sigma^+$  and  $\pi^+\Xi^0$ . Exploring the full 95% confidence interval error ellipse in the  $h$ - $C$  plane

TABLE IX.  $SU(2)$  extrapolated scattering lengths using the LECs from Table VIII. The first uncertainty in parentheses is statistical, and the second is the statistical and systematic uncertainty added in quadrature.

Quantity	LO (fm)	NLO (fm)	NLO (NNLO fit) (fm)	NNLO (fm)
$a_{\pi\Sigma}$	-0.2294	-0.212(03)(04)	-0.190(04)(06)	-0.197(04)(09)
$a_{\pi\Xi}$	-0.1158	-0.106(04)(05)	-0.095(02)(09)	-0.102(02)(09)

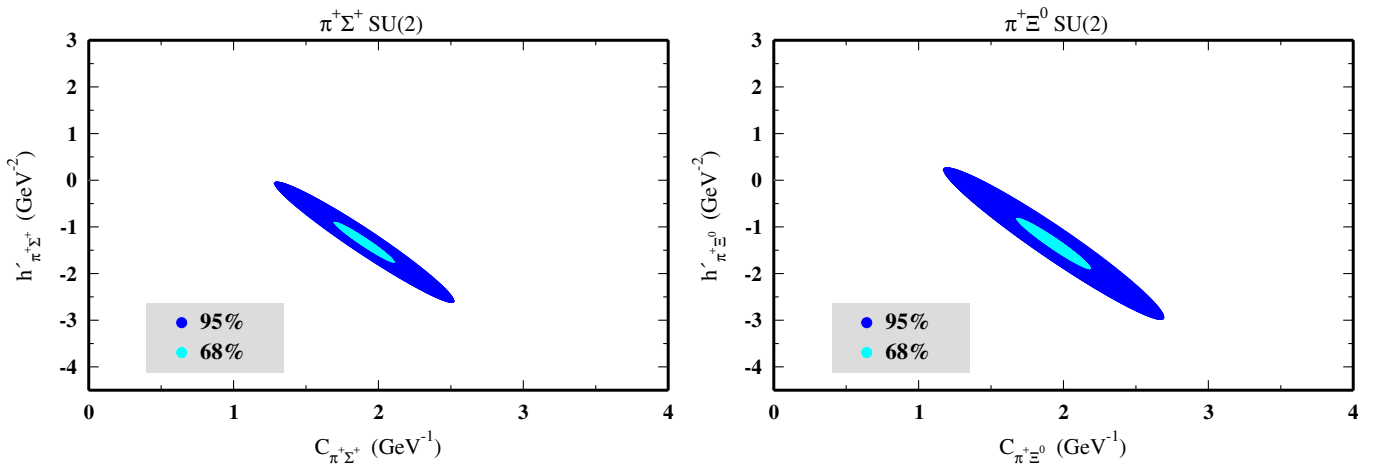


FIG. 10 (color online). The 68% (light) and 95% (dark) confidence interval error ellipses for fits for the  $\pi^+\Sigma^+$  (left), and  $\pi^+\Xi^0$  (right) processes using Eqs. (41) and (42).

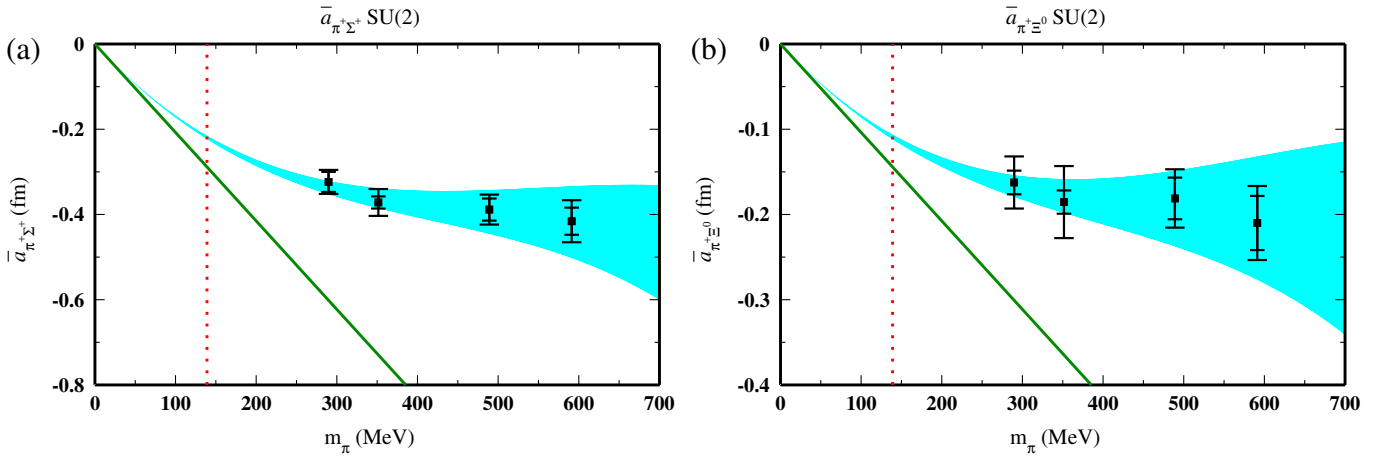


FIG. 11 (color online).  $\bar{a}$  plots for the  $\pi^+\Sigma^+$ , and  $\pi^+\Xi^0$  processes versus the pion mass. The diagonal line is the leading order curve, and the dotted line is the physical pion mass. The innermost error bar is the statistical uncertainty and the outermost error bar is the statistical and systematic uncertainty added in quadrature. The filled bands are the fits to the LECs in the  $SU(2)$  case at NNLO as in Eqs. (45) and (46).

yields

$$a_{\pi^+\Sigma^+} = -0.197 \pm 0.011 \text{ fm}; \quad (43)$$

$$a_{\pi^+\Xi^0} = -0.102 \pm 0.004 \text{ fm}. \quad (44)$$

Comparison of these determinations with those of Eq. (40) give an estimate of the systematic error due to truncation of the chiral expansion at order  $m_\pi^3$ . We have also ‘‘pruned’’ the data; that is, we have redone all fits omitting the heaviest mass ensemble. While this procedure inflates the errors, we see very little shift in the central values.

In order to plot the scattering length versus  $m_\pi$ , we define

$$\begin{aligned} \bar{a}_{\pi^+\Sigma^+} &= a_{\pi^+\Sigma^+} \left( \frac{m_\pi + m_\Sigma}{m_\Sigma} \right) \\ &= \frac{1}{2\pi} \left( -\frac{m_\pi}{f^2} + \frac{m_\pi^2}{f^2} C_{\pi^+\Sigma^+} + \frac{m_\pi^3}{f^2} h'_{\pi^+\Sigma^+} \right); \end{aligned} \quad (45)$$

$$\begin{aligned} \bar{a}_{\pi^+\Xi^0} &= a_{\pi^+\Xi^0} \left( \frac{m_\pi + m_\Xi}{m_\Xi} \right) \\ &= \frac{1}{4\pi} \left( -\frac{m_\pi}{f^2} + \frac{m_\pi^2}{f^2} C_{\pi^+\Xi^0} + \frac{m_\pi^3}{f^2} h'_{\pi^+\Xi^0} \right). \end{aligned} \quad (46)$$

In Fig. 11 we plot the scattering lengths versus the pion mass. The shaded bands in these plots correspond to the standard error in the determination of the LECs, as given in Table VIII.

Additional systematic errors arising from the specific lattice formulation that we employ are discussed in detail in Ref. [1], and are expected to be well-encompassed by our error bars. As discussed in Sec. III, there is a systematic error in extracting the scattering length from the phase shift. We find that range corrections affect the scattering length at the 5% level for  $\pi^+\Sigma^+$ , and at the 1% level for  $\pi^+\Xi^0$ . Finally, we reiterate that there are unquantified

systematic errors due to finite-volume and lattice-spacing effects, however, these errors are likely encompassed by our quoted errors.

## VIII. CONCLUSIONS

In this paper we have presented the first fully-dynamical lattice QCD calculation of meson-baryon scattering. While the phenomenologically most-interesting case of pion-nucleon scattering involves annihilation diagrams, and therefore, requires more resources than we currently have available, we have calculated the ground-state energies of  $\pi^+\Sigma^+$ ,  $\pi^+\Xi^0$ ,  $K^+p$ ,  $K^+n$ , and  $K^0\Xi^0$ , which involve no annihilation diagrams.

An analysis of the scattering lengths of these two-body systems using HB $\chi$ PT has led us to conclude that the three-flavor chiral expansion does not converge over the range of light-quark masses that we investigate. While the kaon-baryon scattering lengths appear perturbative at NLO, a comparison of NNLO with NLO calls into question the convergence of the three-flavor chiral expansion. Therefore, we do not quote values for the kaon-baryon scattering lengths at the physical point. On the other hand, the  $\pi^+\Sigma^+$  and  $\pi^+\Xi^0$  scattering lengths appear to have a well-controlled chiral expansion in two-flavor HB $\chi$ PT. Our results,  $a_{\pi^+\Sigma^+} = -0.197 \pm 0.017$  fm, and  $a_{\pi^+\Xi^0} = -0.098 \pm 0.017$  fm, deviate from the LO (current algebra) predictions at the one- and two-sigma level, respectively. We look forward to confirmation of these predictions from other lattice QCD calculations and possibly from future experiments.

The HB $\chi$ PT analyses performed in this work support a general observation about convergence in the three-flavor chiral expansion, at least for the processes studied here. As the pion masses considered in this lattice calculation are comparable to the physical kaon mass, the distinct con-

vergence patterns of the two- and three-flavor chiral expansions found in this work are suggestive that the breakdown in the three-flavor case is not due to the relative largeness of the strange-quark mass as compared to the light-quark masses, but rather due to some other enhancement in the coefficients of the loop contributions, possibly related to a scaling with powers of  $n_f$ , the number of flavors.

While in this paper we have not considered the lowest-lying baryon decuplet, one interesting process for future study is the  $\pi^- \Omega^-$  system. It does not involve disconnected diagrams since the pions have no valence quarks with the same flavor as the  $\Omega^-$  constituents. It has been argued that there is a bound state [70] in this channel, and therefore, it would be of interest to determine whether this state appears bound on the lattice at the available quark masses.

### ACKNOWLEDGMENTS

We thank U.G. Meißner for useful discussions, and R. Edwards and B. Joo for help with the QDP++/Chroma programming environment [71] with which the calculations discussed here were performed. We gratefully acknowledge the computational time provided by NERSC (Office of Science of the U.S. Department of Energy, No. DE-AC02-05CH11231), the Institute for Nuclear Theory, Centro Nacional de Supercomputación

(Barcelona, Spain), Lawrence Livermore National Laboratory, and the National Science Foundation through Teragrid resources provided by the National Center for Supercomputing Applications and the Texas Advanced Computing Center. Computational support at Thomas Jefferson National Accelerator Facility and Fermi National Accelerator Laboratory was provided by the USQCD collaboration under *The Secret Life of a Quark*, a U.S. Department of Energy SciDAC project (<http://www.scidac.gov/physics/quarks.html>). The work of M.J.S. was supported in part by the U.S. Department of Energy under Grant No. DE-FG03-97ER4014. The work of K.O. and W.D. was supported in part by the U.S. Department of Energy contract No. DE-AC05-06OR23177 (JSA) and DOE grant DE-FG02-04ER41302. K.O. and A.W.L. were supported in part by the Jeffress Memorial Trust, grant J-813 and DOE OJI grant DE-FG02-07ER41527. The work of S.R.B. and A.T. was supported in part by the National Science Foundation CAREER grant No. PHY-0645570. Part of this work was performed under the auspices of the US DOE by the University of California, Lawrence Livermore National Laboratory under Contract No. W-7405-Eng-48. The work of A.P. was partly supported by the EU contract FLAVIANet MRTN-CT-2006-035482, by the contract FIS2008-01661 from MEC (Spain) and FEDER and by the Generalitat de Catalunya contract 2005SGR-00343.

- 
- [1] S.R. Beane, T.C. Luu, K. Orginos, A. Parreño, M.J. Savage, A. Torok, and A. Walker-Loud, *Phys. Rev. D* **77**, 014505 (2008).
- [2] S.R. Beane, P.F. Bedaque, T.C. Luu, K. Orginos, E. Pallante, A. Parreño, and M.J. Savage, *Phys. Rev. D* **74**, 114503 (2006).
- [3] S.R. Beane, T.C. Luu, K. Orginos, A. Parreño, M.J. Savage, A. Torok, and A. Walker-Loud (NPLQCD Collaboration), *Phys. Rev. D* **77**, 094507 (2008).
- [4] S.R. Beane, W. Detmold, T.C. Luu, K. Orginos, M.J. Savage, and A. Torok, *Phys. Rev. Lett.* **100**, 082004 (2008).
- [5] W. Detmold, M.J. Savage, A. Torok, S.R. Beane, T.C. Luu, K. Orginos, and A. Parreno, *Phys. Rev. D* **78**, 014507 (2008).
- [6] W. Detmold, K. Orginos, M.J. Savage, and A. Walker-Loud, *Phys. Rev. D* **78**, 054514 (2008).
- [7] For a recent review, see V. Bernard, *Prog. Part. Nucl. Phys.* **60**, 82 (2008).
- [8] S.R. Beane, P.F. Bedaque, K. Orginos, and M.J. Savage, *Phys. Rev. Lett.* **97**, 012001 (2006).
- [9] S.R. Beane, P.F. Bedaque, T.C. Luu, K. Orginos, E. Pallante, A. Parreño, and M.J. Savage (NPLQCD Collaboration), *Nucl. Phys.* **A794**, 62 (2007).
- [10] S.R. Beane *et al.*, *Phys. Rev. D* **79**, 114502 (2009).
- [11] G.P. Lepage, “The Analysis Of Algorithms For Lattice Field Theory,” Invited lectures given at TASI’89 Summer School, Boulder, CO, 1989.
- [12] D.B. Kaplan, M.J. Savage, and M.B. Wise, *Nucl. Phys.* **B534**, 329 (1998).
- [13] See, for instance, R. Babich, R. Brower, M. Clark, G. Fleming, J. Osborn, and C. Rebbi, *Proc. Sci., LATTICE2008* (2008) 160 [arXiv:0901.4569].
- [14] E. E. Jenkins and A. V. Manohar, *Phys. Lett. B* **255**, 558 (1991).
- [15] Y.R. Liu and S.L. Zhu, *Phys. Rev. D* **75**, 034003 (2007).
- [16] Y.R. Liu and S.L. Zhu, *Eur. Phys. J. C* **52**, 177 (2007).
- [17] N. Kaiser, *Phys. Rev. C* **64**, 045204 (2001); **73**, 069902 (2006).
- [18] M. Mai, P.C. Bruns, B. Kubis, and U.G. Meißner, *Phys. Rev. D* **80**, 094006 (2009).
- [19] D.B. Kaplan and A.E. Nelson, Report No. HUTP-86/A023; *Phys. Lett. B* **175**, 57 (1986); **192**, 193 (1987); *Nucl. Phys.* **A479**, 273 (1988); **A479**, 285 (1988).
- [20] M. Lu, M.B. Wise, and M.J. Savage, *Phys. Lett. B* **337**, 133 (1994).
- [21] H.C. Schroder *et al.*, *Phys. Lett. B* **469**, 25 (1999).
- [22] H.C. Schroder *et al.*, *Eur. Phys. J. C* **21**, 473 (2001).
- [23] A.D. Martin, *Nucl. Phys.* **B179**, 33 (1981).
- [24] M. Fukugita, Y. Kuramashi, M. Okawa, H. Mino, and A.

- Ukawa, *Phys. Rev. D* **52**, 3003 (1995).
- [25] G. w. Meng, C. Miao, X. n. Du, and C. Liu, *Int. J. Mod. Phys. A* **19**, 4401 (2004).
- [26] S. Weinberg, *Phys. Rev. Lett.* **17**, 616 (1966).
- [27] B. C. Tiburzi, *Phys. Rev. D* **72**, 094501 (2005).
- [28] J. W. Chen, D. O'Connell, and A. Walker-Loud, *J. High Energy Phys.* **04** (2009) 090.
- [29] J. W. Chen, D. O'Connell, R. S. Van de Water, and A. Walker-Loud, *Phys. Rev. D* **73**, 074510 (2006).
- [30] J. W. Chen, D. O'Connell, and A. Walker-Loud, *Phys. Rev. D* **75**, 054501 (2007).
- [31] S. R. Beane, K. Orginos, and M. J. Savage, *Int. J. Mod. Phys. E* **17**, 1157 (2008).
- [32] K. Huang and C. N. Yang, *Phys. Rev.* **105**, 767 (1957); H. W. Hamber, E. Marinari, G. Parisi, and C. Rebbi, *Nucl. Phys.* **B225**, 475 (1983); M. Lüscher, *Commun. Math. Phys.* **105**, 153 (1986); *Nucl. Phys.* **B354**, 531 (1991).
- [33] S. R. Beane, P. F. Bedaque, A. Parreño, and M. J. Savage, *Phys. Lett. B* **585**, 106 (2004).
- [34] D. B. Kaplan, *Phys. Lett. B* **288**, 342 (1992).
- [35] Y. Shamir, *Phys. Lett. B* **305**, 357 (1993).
- [36] Y. Shamir, *Nucl. Phys.* **B406**, 90 (1993).
- [37] V. Furman and Y. Shamir, *Nucl. Phys.* **B439**, 54 (1995).
- [38] Y. Shamir, *Phys. Rev. D* **59**, 054506 (1999).
- [39] K. Orginos, D. Toussaint, and R. L. Sugar, *Phys. Rev. D* **60**, 054503 (1999).
- [40] K. Orginos and D. Toussaint, *Phys. Rev. D* **59**, 014501 (1998).
- [41] C. W. Bernard *et al.*, *Phys. Rev. D* **64**, 054506 (2001).
- [42] S. R. Beane, P. F. Bedaque, K. Orginos, and M. J. Savage (NPLQCD Collaboration), *Phys. Rev. D* **73**, 054503 (2006).
- [43] W. Schroers *et al.* (LHPC Collaboration and SESAM Collaboration), *Nucl. Phys. B, Proc. Suppl.* **129**, 907 (2004).
- [44] A. Hasenfratz and F. Knechtli, *Phys. Rev. D* **64**, 034504 (2001).
- [45] T. A. DeGrand, A. Hasenfratz, and T. G. Kovacs, *Phys. Rev. D* **67**, 054501 (2003).
- [46] T. A. DeGrand, *Phys. Rev. D* **69**, 014504 (2004).
- [47] M. Creutz, [arXiv:hep-lat/0603020](https://arxiv.org/abs/hep-lat/0603020).
- [48] C. Bernard, *Phys. Rev. D* **73**, 114503 (2006).
- [49] C. Bernard, M. Golterman, Y. Shamir, and S. R. Sharpe, *Phys. Lett. B* **649**, 235 (2007).
- [50] M. Creutz, *Phys. Lett. B* **649**, 241 (2007).
- [51] C. Bernard, M. Golterman, and Y. Shamir, *Phys. Rev. D* **73**, 114511 (2006).
- [52] C. Bernard, M. Golterman, and Y. Shamir, *Proc. Sci., LAT2006* (2006) 205 [[arXiv:heplat/0610003](https://arxiv.org/abs/heplat/0610003)].
- [53] M. Creutz, *Phys. Lett. B* **649**, 230 (2007).
- [54] M. Creutz, *Phys. Lett. B* **649**, 241 (2007).
- [55] S. Dürr, C. Hoelbling, and U. Wenger, *Phys. Rev. D* **70**, 094502 (2004).
- [56] S. Dürr and C. Hoelbling, *Phys. Rev. D* **71**, 054501 (2005).
- [57] S. Dürr and C. Hoelbling, *Phys. Rev. D* **74**, 014513 (2006).
- [58] A. Hasenfratz and R. Hoffmann, *Phys. Rev. D* **74**, 014511 (2006).
- [59] Y. Shamir, *Phys. Rev. D* **75**, 054503 (2007).
- [60] S. R. Sharpe, *Proc. Sci., LAT2006* (2006) 022 [[arXiv:hep-lat/0610094](https://arxiv.org/abs/hep-lat/0610094)].
- [61] G. Dahlquist and Å. Björck, *Numerical Methods* (Prentice-Hall, Englewood Cliffs, NJ, 1974), 1st ed.
- [62] S. R. Beane *et al.*, *Phys. Rev. D* **80**, 074501 (2009).
- [63] C. Michael, *Nucl. Phys.* **B259**, 58 (1985).
- [64] M. Luscher and U. Wolff, *Nucl. Phys.* **B339**, 222 (1990).
- [65] W. Detmold and M. J. Savage, *Nucl. Phys.* **B743**, 170 (2004).
- [66] S. He, X. Feng, and C. Liu, *J. High Energy Phys.* **07** (2005) 011.
- [67] K. Orginos and A. Walker-Loud, *Phys. Rev. D* **77**, 094505 (2008).
- [68] H. W. Lin and K. Orginos, *Phys. Rev. D* **79**, 034507 (2009).
- [69] G. Colangelo, J. Gasser, and H. Leutwyler, *Nucl. Phys.* **B603**, 125 (2001).
- [70] W. L. Wang, F. Huang, Z. Y. Zhang, Y. W. Yu, and F. Liu, *Eur. Phys. J. A* **32**, 293 (2007).
- [71] R. G. Edwards and B. Joo (SciDAC Collaboration and LHPC Collaboration and UKQCD Collaboration), *Nucl. Phys. B, Proc. Suppl.* **140**, 832 (2005).